

**STRUCTURAL INSIGHTS INTO THE DNA BINDING ACTIVITY OF
METALLOREGULATOR FUR IN *CAMPYLOBACTER JEJUNI***

François Charih

A thesis submitted to the
Faculty of Medicine
in partial fulfillment of the requirements for the course
BCH4040 - Honours Research Project

Department of Biochemistry, Microbiology and Immunology
Faculty of Medicine

University of Ottawa
© François Charih, 2015

Abstract

Campylobacteriosis is among the leading causes of diarrheal illnesses in humans and is linked to the pathogenesis of debilitating autoimmune disorders. *Campylobacter jejuni*, the major etiological factor causing campylobacteriosis, must cope with the variable bioavailability of iron in the gastrointestinal tract of animals and maintain appropriate iron homeostasis to survive and proliferate, as excessive iron concentrations promote the synthesis of deleterious reactive oxygen species. The transcription factor Ferric Uptake Regulator (Fur) acts as a sensor and regulator of intracellular iron content, and activates or represses the expression of genes involved in iron homeostasis as well as oxidative stress response. Evidence shows that the iron-free (apo) and iron-loaded (holo) forms of Fur generally interact with different DNA motifs in the promoters of Fur-regulated genes. Our previous structural studies have shown that apo-CjFur forms a V-shaped dimer, and that each monomer comprises a DNA binding domain (DBD) and a dimerization domain (DD) connected by a hinge region. The disposition of the apo-CjFur DBD is peculiar when compared with that of previously characterized holo-Fur homologs. Close inspection of the crystal structure revealed that remnants of the tag used to purify apo-CjFur engage in strong interactions with the DD raising the possibility that these extraneous residues may “lock” the DBD of apo-CjFur in its atypical orientation. To address this problem, we engaged in structural studies using a different tagging strategy. The new crystal structure of Fur reveals no apparent differences with the previously solved structure demonstrating that the initial tagging approach did not force the peculiar conformation observed in our initial structural studies. Overall, our findings provide further evidence towards the existence of the apo form of CjFur and provide useful data for drug design applications.

Acknowledgements

First, I wish to thank Prof. Jean-François Couture for his trust and guidance over the last year. I am also very grateful for his patience and his helping hand, especially as this project neared its end. His passion, his drive and his humility as a scientist are inspiring. His ability to see success where other people see failure is truly amazing as well.

Next, I would like to express my gratitude to Sabina Sarvan who generously accepted to be my mentor me on a daily basis. I am indebted to her for teaching me so much about science, but also for, unbeknownst to her, teaching me invaluable lessons about perseverance and hard work. She is an admirable scientist, but also an admirable person and friend.

I also wish to thank Sylvain Lanouette for his wisdom, his help and for our too few, but fascinating conversations on future opportunities and job seeking. I will keep fond memories of Sylvain as a door opener and an opportunity bearer.

I will remember all the other members of the Couture lab who made this experience such an enjoyable one: Véronique Tremblay, John Haddad, Pamela Zhang, Elisa Bergamin and Josée Malette.

Finally, I thank my family for believing in me and for their unconditional support. I owe them everything...

Table of Contents

| | |
|--|------------|
| Abstract..... | II |
| Acknowledgements | III |
| Table of Contents | IV |
| List of Figures..... | VI |
| List of Tables | VI |
| Statement of Contributions..... | VII |
| Experimental Conception..... | VII |
| Manuscript Redaction | VII |
| Experimental Procedures and Data Analysis..... | VII |
| 1. Introduction | 8 |
| 2. Materials and Methods | 16 |
| 2.1. The pStrep-CjFur WT construct..... | 16 |
| 2.2. Overexpression of CjFur WT | 16 |
| 2.3. Purification of CjFur WT | 17 |
| 2.4. Screening of Crystallization Conditions for Apo-CjFur | 18 |
| 2.5. Initial X-Ray Diffraction Experiments for Apo-CjFur | 19 |
| 2.6. Optimization of Crystallization Conditions for Apo-CjFur | 19 |
| 2.7. Final X-Ray Diffraction Experiments for Apo-CjFur..... | 19 |
| 2.8. Resolution of the Apo-CjFur Crystal Structure | 20 |
| 2.9. Screening Crystallization Conditions for the Holo-CjFur-DNA Complex..... | 20 |
| 2.10. Generation of the CjFur R14E and K17E Mutants | 21 |

| | |
|---|-----------|
| 2.11. <i>In Vitro</i> Characterization of the R14E and K17E Mutants..... | 22 |
| 3. Results..... | 24 |
| 3.1. Purification of CjFur WT | 24 |
| 3.2. Crystallization of Apo-CjFur..... | 27 |
| 3.3. Crystal Structure of Apo-CjFur | 29 |
| 3.4. Comparative analysis of the apo-CjFur structures obtained with different tagging strategies | 34 |
| 3.5. Crystallization of the Holo-CjFur-DNA Complex..... | 36 |
| 3.6. <i>In Vitro</i> Characterization of the CjFur R14E and K17E Mutants..... | 38 |
| 4. Discussion | 40 |
| 5. References..... | 45 |
| 6. Appendices | 51 |
| 6.1. Appendix A: The pStrep-CjFur WT Construct..... | 51 |
| 6.2. Appendix B: Crystallization of Apo-CjFur | 52 |
| 6.3. Appendix C: Crystallization of the Holo-CjFur-DNA complex | 52 |
| 6.4. Appendix D: <i>In Vitro</i> Characterization of the CjFur R14E and K17E mutants | 55 |

List of Figures

| | |
|--|----|
| Figure 1. The first apo-CjFur structure solved by X-ray crystallography | 11 |
| Figure 2. Orientations of the DNA binding domain across Fur homologs..... | 12 |
| Figure 3. Interactions between the SUMO tag remnants and the dimerization domain of apo-CjFur | 13 |
| Figure 4. Purification of CjFur WT | 26 |
| Figure 5. Crystals and diffraction pattern of the new apo-CjFur construct | 28 |
| Figure 6. Crystal Structure of the new apo-CjFur construct..... | 31 |
| Figure 7. Ramachandran plot of the new apo-CjFur model..... | 32 |
| Figure 8. The S1 metal binding site in the new apo-CjFur crystal structure | 33 |
| Figure 9. Structural alignment of the old and new CjFur crystal structures | 35 |
| Figure 10. Crystals obtained following crystallization screenings with the holo-CjFur-DNA complex..... | 37 |
| Figure 11. Characterization of the holo-CjFur R14E and K17E mutants by EMSA..... | 39 |
| Figure 12. The constructs used to purify and solve the crystal structure of apo-CjFur..... | 51 |
| Figure 13. Custom-made crystallization screening kit | 52 |

List of Tables

| | |
|---|----|
| Table 1. List of DNA oligonucleotides screened for the crystallization of the holo-CjFur-DNA complex..... | 52 |
| Table 2. List of crystallization screening kits used for crystallization experiments | 54 |

Statement of Contributions

Experimental Conception

Prof. Jean-François Couture (JFC) and Sabina Sarvan (SS) conceived all the experiments. SS was responsible for the conception and optimization of the CjFur purification protocol, the Electrophoretic Mobility Shift Assay, and the site-directed mutagenesis conditions. SS and JFC conceived the oligonucleotides for the crystallization experiments involving the holo-CjFur-DNA complex. François Charih (FC) conceived the optimization experiments for the crystallization of apo-CjFur and the holo-CjFur-DNA complex.

Manuscript Redaction

This manuscript was written by FC with the assistance of JFC who reviewed the document, provided comments as well as recommendations and helped with the editing. SS provided additional help and provided FC with some guidance in his literature review.

Experimental Procedures and Data Analysis

SS and JFC conceived and generated the pStrep-CjFur protein construct before FC's arrival in May 2014. FC performed all experiments except for the X-ray diffraction experiments involving apo-CjFur which and the EMSA procedure for holo-CjFur WT which were performed by SS. The holo-CjFur hypothetical molecular model (Figure 11A) was built by SS. The final data collection and the initial modeling for the new apo-CjFur structure was done by Joseph Brunzelle (JB). FC built and refined the apo-CjFur crystal structure and generated the figures with assistance from JFC. JFC performed the structural alignment of the two apo-CjFur crystal structures. All data was analyzed by FC under SS and JFC's supervision.

1. Introduction

Campylobacter jejuni is one of the principal pathological organism causing gastroenteritis worldwide (Kaakoush et al., 2015). This gram-negative, microaerophilic prokaryote colonizes the gastrointestinal tracts of humans and causes acute, but generally self-limiting symptoms in humans including bloody diarrhea, fever, weight loss and cramps (Kaakoush et al., 2015). In addition to directly causing gastroenteritis, which may follow exposure to contaminated poultry products (Friedman et al., 2004), campylobacteriosis has been found to be a common event preceding the pathogenesis of other, more serious and debilitating conditions including the Guillain-Barré Syndrome (GBS) (Gibney et al., 2014; Godschalk et al., 2004; Mishu et al., 1993). GBS is a severe, life-threatening autoimmune condition that causes an ascending paralysis of the limbs and impairment of the autonomic nervous system (Dash et al., 2014). Associations with other chronic diseases have also been established. For instance, there are reports of *C. jejuni*'s involvement in the development or exacerbation of irritable bowel syndromes (Qin et al., 2011), reactive arthritis (Pope et al., 2007) and the Miller-Fisher Syndrome (Salloway et al., 1996), among others.

Like almost all forms of life, *C. jejuni* has an absolute requirement for iron (Fillat, 2014). Iron is an essential constituent of various proteins such as heme-proteins and iron-sulfur cluster proteins and confers them the appropriate redox potential necessary for proper protein function (Andrews et al., 2003). The cellular processes in which iron is involved in bacteria are numerous and include energy metabolism, DNA biosynthesis, oxygen transport, and redox reactions (Andrews et al., 2003; Braun, 2001; Fillat, 2014; Troxell and Hassan, 2013). Iron is also a major player in the host-pathogen interactions, as iron has been demonstrated to play a crucial role in the expression of important virulence factors affecting protein glycosylation, flagellar motility, chemotaxis and adhesion in *C. jejuni* (Palyada et al., 2004; Van Vliet et al., 2002).

The bioavailability of iron in the gastrointestinal tract is highly variable and correlates with the changes in pH, oxygen levels, and redox status in this complex environment (Wooldridge and Vliet, 2005). Under oxidizing conditions, iron exists mostly in the ferric form (Fe^{3+}) which is virtually insoluble and therefore not accessible to living organisms (Wooldridge and Vliet, 2005). Furthermore, hosts are known to restrict the concentrations of free iron in order to prevent the survival and proliferation of undesirable microorganisms (Butcher et al., 2010).

To overcome the challenges associated with the low, but variable bioavailability of iron, bacteria have devised multiple iron uptake systems that rely on the chelation or reduction of insoluble ferric iron to increase its solubility (Andrews et al., 2003). In particular, *C. jejuni* has been shown to express a variety of transmembrane transporters that allow the uptake the cell of iron conjugated to a variety of exogenous siderophores, low molecular weight chelating agents that have the ability to bind and solubilize Fe^{3+} to facilitate its transport into the cell (Miller et al., 2009). More specifically, *C. jejuni* has been shown to rely on siderophores which include enterobactin and enantioenterobactin (Abergel et al., 2009) as well as lactoferrin and members of the transferrin family (Miller et al., 2008). *C. jejuni* also scavenges for iron by internalizing heme-bound iron (Ridley et al., 2006).

Although iron is indispensable in *C. jejuni*, its intracellular concentrations must be tightly regulated. Aberrantly high concentrations of iron are harmful to the cell as iron is known to undergo the Fenton and Haber-Weiss reactions to produce the cytotoxic hydroxyl radical (OH^-) which increases oxidative stress and damages biomacromolecules through oxidation (Imlay et al., 1988; Lloyd et al., 1997).

The ubiquitous prokaryotic transcription factor Ferric Uptake Regulator (Fur) is considered the main regulator of iron in gram-negative bacteria (Butcher et al., 2010; Fillat, 2014). The role

of Fur as a regulator of intracellular iron content was first identified in *E. coli* (Hantke, 1981). Fur is viewed as the central member of the FUR superfamily of metalloregulators which now encompasses a set of proteins sharing at least some similar structural and functional features and involved in the uptake and homeostasis of iron and other metals such as manganese (Mur), nickel (Nur), and zinc (Zur) (Fillat, 2014; Lee and Helmann, 2007).

Fur employs a variety of mechanisms to fulfill one of its main roles: to probe, and ultimately, to regulate intracellular iron levels (Fillat, 2014; Lee and Helmann, 2007; Troxell and Hassan, 2013). The classical Fur regulation model specified that under iron-replete conditions, iron binds to the iron-free (apo) Fur and induces a conformational change that promotes the binding of the iron-bound (holo) Fur to its DNA target to repress expression of genes downstream (Bagg and Neilands, 1987; Lavrrar et al., 2002). A large portion of these Fur-regulated genes encodes proteins involved in transport of iron and other inorganic ions (Butcher et al., 2012; Palyada et al., 2009). It is now known that this model is incomplete and that Fur regulates gene expression using additional mechanisms (Lee and Helmann, 2007). Indeed, there is now a body of evidence suggesting that Fur, in *Campylobacter jejuni* and *Helicobacter pylori*, activates and represses gene expression, both under iron-replete (holo-regulation) and iron-deplete conditions (apo-regulation) (Butcher and Stintzi, 2013; Butcher et al., 2012; Ernst et al., 2005).

The crystal structure of the apo form of Fur in *C. jejuni* (apo-CjFur) published by Butcher et al., 2012 (PDB: 4ETS) has provided invaluable insight into the overall structure of the protein, and details regarding how CjFur may respond to varying iron concentrations and bind to the Fur-box in *C. jejuni*. Like other Fur proteins, apo-CjFur forms two domains upon folding; a DNA binding domain (DBD) located in the N-terminus of the protein, and a dimerization domain (DD) on its C-terminus (Figure 1). The DBD comprises five α -helices followed by two β -sheets while

the DD consists of 3 β -sheets and 2 α -helices. An 8-residue long hinge region connects the two domains. The crystal structure also revealed that apo-CjFur dimerizes in solution and assumes the canonical V-shaped conformation, which is commonly encountered in other holo-Fur proteins.

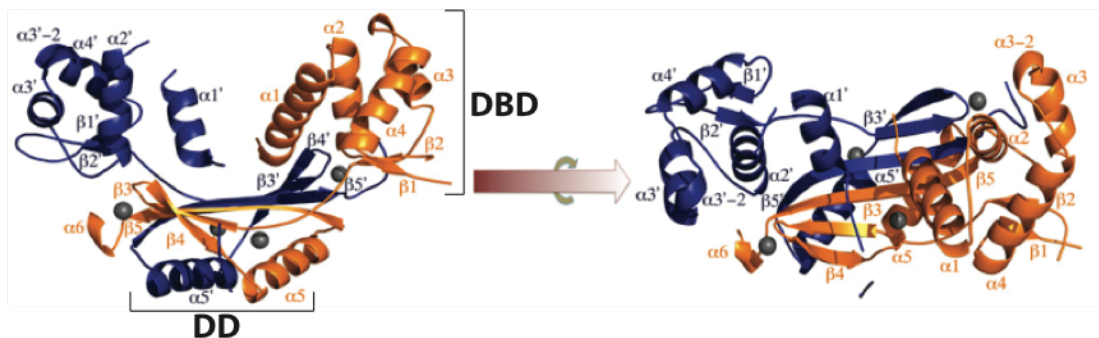


Figure 1. The first apo-CjFur structure solved by X-ray crystallography

The crystal structure of apo-CjFur solved at 2.1 \AA resolution. Shown are two orthogonal views of the apo-CjFur crystal structure. The DNA binding domains (DBD) and dimerization domains are labeled. (Adaptation of Figure 3 in Butcher et al., 2012a.)

Each protomer in the apo-CjFur structure coordinates two zinc atoms. Fur was previously shown to coordinate zinc atoms in other species including *Vibrio cholerae* (Sheikh and Taylor, 2009), *Pseudomonas aeruginosa* (Pohl et al., 2003) and *Helicobacter pylori* (Dian et al., 2011). In CjFur, the zinc atoms are coordinated in the site S1 located in the DD domain of the protein and in the site S3 located at the C-terminus end of the hinge region. In the site S1, zinc is tetra-coordinated by a common CXXC tetra-cysteine zinc binding motif found in many Fur proteins (Fillat, 2014; Lee and Helmann, 2007), whereas in site S3, zinc is penta-coordinated by three residues (D101, E120, H137) and two water molecules. The current understanding is that the zinc atoms bound in the coordination sites play a structural role and ensure proper protein folding and dimerization as demonstrated with mutational studies in HpFur, CjFur's closest homolog in *H. pylori* (Butcher et al., 2012; Dian et al., 2011). There remains some controversy regarding the role

of the zinc atoms, however, as zinc atoms in the VcFur and PaFur structures were shown to be dispensable and to not play a role in maintaining the structural integrity of the protein (Lewin et al., 2002; Sheikh and Taylor, 2009). A third regulatory metal binding site, S2, is thought to trigger the conformational change responsible for the shift from apo-regulation to holo-regulation upon metal binding in *C. jejuni* (Butcher et al., 2012). The apo-CjFur structure DBD places the residues presumed to be involved in the coordination of the regulatory iron in a conformation which cannot allow metal coordination (Butcher et al., 2012).

Apo-CjFur sets itself apart from the other Fur and Fur-like proteins in at least two important ways. First, in contrast with the apo structure of BsPerR, a paralog of Fur in *B. subtilis*, apo-CjFur assumes a V-shaped conformation whereas apo-BsPerR assumes a quasi-planar conformation (Traoré et al., 2006). Indeed, the overall conformation of CjFur's overall conformation is closer to that of other Holo-Fur proteins than to that of apo-BsPerR, the only other apo structure deposited in the RCSB Protein Databank as of now. Second, the DBD of apo-CjFur appears to be rotated by 180° in relationship with the holo form of HpFur, VcFur and PaFur, and orients the α 1 helix towards the inside of protein concavity (Figure 2).

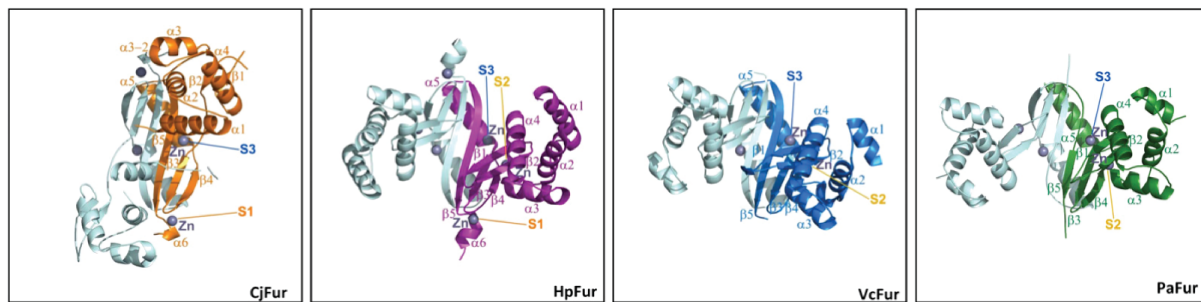


Figure 2. Orientations of the DNA binding domain across Fur homologs

Shown are the crystal structures of Fur homologs in *Campylobacter jejuni* (CjFur), *Helicobacter pylori* (HpFur, PDB: 2XIG), *Vibrio cholerae* (VcFur, PDB: 2W57) and *Pseudomonas aeruginosa* (PaFur, PDB: 1MZB), as viewed from the above the V-cleft. Secondary structures in one of the monomers are labeled in each structure. (Adaptation of Figure S3 in Butcher et al., 2012.)

Two explanations have been provided for the peculiar orientation of the DBD in apo-CjFur. First, the crystal structure of apo-CjFur showed that remnants of the SUMO tag (4 residues) used for purification and solubility purposes were appended at the N-terminus end of the wild-type protein. Additional analyses have shown that these additional residues can engage in strong interactions with the DD of the protein, possibly “locking” apo-CjFur into its atypical conformation (Figure 3).

Second, a structural alignment of apo-CjFur with holo-HpFur has revealed that this rotation may be caused by the disposition of the hinge region, which is elongated in apo-CjFur, but bent in holo-HpFur (Butcher et al., 2012). The flexibility of the hinge region and its role in the reorientation of the DBD domain and activation of the DNA binding activity of other transcription factors has been described previously (Lanzilotta et al., 2000; Lucarelli et al., 2007).

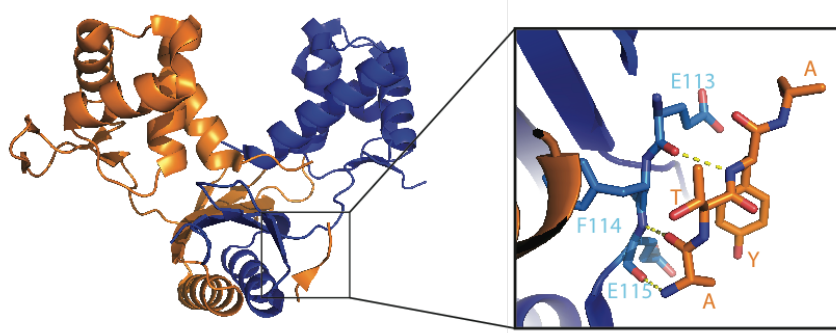


Figure 3. Interactions between the SUMO tag remnants and the dimerization domain of apo-CjFur

Shown is a zoomed view of the interactions between the remnants of the SUMO tag in the crystal structure of apo-CjFur published in Butcher et al., 2012. The residues A-T-Y-A belonging to the remnants are shown as sticks rendered and labeled in orange, while residues from the apo-CjFur DD engaging in the interactions are highlighted and labeled in pale blue.

The DNA motifs recognized by Fur proteins, Fur boxes, are often but not always palindromic and AT-rich (Fillat, 2014; Lee and Helmann, 2007). Consensus sequences for holo-

CjFur binding sites have been published. Holo-CjFur recognizes and binds to the partially palindromic consensus sequence 5'-TATTTGATAATTATTATCA-3' (the 7-1-7 palindromic motif is underlined) and represses the expression of downstream genes (Butcher et al., 2012). Holo-CjFur may also bind to the non-palindromic consensus sequence 5'-TTGGAACANTTTTGCT-3' to activate gene expression (Butcher et al., 2012). No apo-CjFur consensus binding sequences have been published as of now, but work to identify a consensus sequence is underway (personal communication J. Butcher and S. Sarvan).

Until recently, the structural basis for the DNA binding activity of all members of the FUR family of metalloregulators had remained vague at best, with most models relying on computational approaches to characterize the Fur-DNA complex (Dian et al., 2011; Pohl et al., 2003; Tiss et al., 2005). The crystal structure of the EcZur, a paralog of CjFur in *E. coli*, in complex with DNA published very recently (PDB: 4MTD; 4MTE) was the first major work to provide a high resolution, reliable model capable of shedding light onto the intricate details of the interaction between a member of the FUR family and DNA (Gilston et al., 2014). It was shown that the DBD of EcZur inserts itself in the major and minor groove of the DNA to allow interactions between the helix-turn-helix motif binds DNA through interactions between the helix-turn-helix (HTH) motif in EcZur's DBD and the nitrogenous bases and phosphate backbone of the DNA molecule. The resolution of the EcZur-DNA complex crystal structure also allowed the group to identify an EcZur DNA target that could not be characterized through classical bioinformatics. In fact, EcZur was determined to bind to DNA in the promoter region of the *pliG* gene and to repress the expression of this gene which encodes a periplasmic lyzozyme inhibitor in *E. coli*.

The economic burden associated with *Campylobacter* infections and its complications is considerable, and estimated to \$1.75B per year in the U.S. (Batz et al., 2012). Furthermore, there

are recent reports of multidrug-resistant strains of *C. jejuni* (Chen et al., 2010b; Little et al., 2008; Mukherjee et al., 2013). The importance of iron in *C. jejuni* is evident and highlighted by the large set of genes in the bacteria that encode proteins dedicated to iron uptake (Miller et al., 2009). CjFur regulates at least 127 genes through holo regulation in iron replete conditions (Butcher and Stintzi, 2013) and 131 genes through apo regulation in iron deplete conditions (Butcher et al., 2012). Studies evaluating the ability of *C. jejuni* to colonize the gastrointestinal tract of animal models have also shown that some Fur mutants have decreased colonization capabilities (Palyada et al., 2004). Moreover, some groups have raised the idea that Fur could be a potential drug target (Lucarelli et al., 2008; Pich and Merrell, 2013; Sheikh and Taylor, 2009). Overall, this provides a solid rationale for the structural characterization of CjFur and the CjFur-DNA interaction. Additional structural data would be of invaluable help in finding how to most effectively target the protein and develop therapeutic molecules to treat campylobacteriosis.

Consequently, we engaged in structural and mutational studies to further characterize apo-CjFur as well as the holo-CjFur-DNA interaction. First, we sought to show that the unique conformation of the apo-CjFur DBD does not result from the presence of remnants of a purification tag by crystallizing and solving the apo-CjFur crystal structure using a different tagging strategy. Next, we worked to gather additional evidence to support the model in which the DBD of CjFur rotates following the binding of iron in the S2 binding site, which induces a conformational change in the hinge region. Finally, we sought to understand the structural basis underlying the specificity of apo-CjFur and holo-CjFur towards their respective DNA targets.

2. Materials and Methods

2.1. The pStrep-CjFur WT construct

The protein construct used in the experiments is schematized in Appendix A: The pStrep-CjFur WT Construct. The construct was designed such that only a glycine residue remains appended to the protein following tag cleavage.

2.2. Overexpression of CjFur WT

E. coli BL21 Rosetta competent cells (Novagen) were transformed with the pStrep-CjFur WT recombinant vector to express CjFur WT using the heat shock method. The cells were first incubated with the vector during 30 minutes on ice, and then heated to 42°C during 1 min. Following a 2 minutes incubation on ice, LB broth was added to the cells which were then allowed to grow in an incubator-shaker (Excella E24, New Brunswick Scientific) at 37°C and 250 RPM. Cells were then spread on an LB agar plate supplemented with ampicillin and chloramphenicol and grown overnight at 37°C in an incubator (Boeckel Scientific).

The following day, a pre-culture in LB broth containing 0.1 mg/mL ampicillin and chloramphenicol was inoculated with the transformants and let grow in the incubator-shaker until it reached a reasonable turbidity. Larger 0.5 L cultures in LB containing identical antibiotic concentrations were inoculated with the pre-culture for the overexpression and incubated in a dedicated incubator-shaker (Innova 43, New Brunswick Scientific) at 37°C and 250 RPM until the OD₆₀₀ measured by spectrophotometry (Biochrom Novaspec Plus, Fischer Scientific) reached approximately 0.4 - 0.5. Temperature was decreased to 18°C, and overnight overexpression was induced using 0.1 mM β-D-1-thiogalactopyranoside (IPTG) (Sigma).

Finally, the cells were harvested by centrifugation (Avanti J25, Beckman Coulter) during 30 mins at 3000 RPM and 4°C. The cell pellets were then resuspended in buffer A (50 mM Tris pH 7.0, 100 mM NaCl, 5 mM β-mercaptoethanol) and stored at -80°C.

2.3. Purification of CjFur WT

Frozen pellets of harvested cells were thawed gently in cold water, and the pellet was further resuspended in buffer A. The cells were lysed on ice three times with 1 minute rounds of sonication (Misonix Sonicator 3000). The crude extract was clarified by high speed centrifugation (Avanti J25 Centrifuge, Beckman Coulter) during 30 minutes at 16 000 RPM and 4°C. The supernatant was filtered on ice using 0.45 µm filters to remove cell debris and large contaminants and applied on an affinity chromatography column packed with Strep-Tactin resin (Qiagen), and pre-equilibrated with 3 column volumes (CV) of buffer A. The bound protein was washed with another 3 CV of buffer A, and was eluted from the resin in ~35 mL buffer A supplemented with 2.5 mM D-desthiobiotin (Sigma). The protein was then dialyzed during 16h at 4°C in presence of the Tobacco Etch Virus (TEV) protease in a 10K MWCO dialysis bag (Thermo Scientific) against 2L of cleavage buffer (50 mM Tris pH 7.0, 250 mM NaCl, 5 mM β-mercaptoethanol) to cleave off the Strep-Tag at the N-terminal end of CjFur.

The cleaved protein was concentrated to ~1.5 mL using a 10K MWCO concentrator (EMD Millipore) and purified by size-exclusion/gel filtration chromatography on a preparative grade Superdex S75 column (GE Healthcare) using an AKTA FPLC system (GE Healthcare). The gel filtration was performed at 4°C in a gel filtration buffer (20 mM Tris pH 7.0, 250 mM NaCl and 5 mM β-mercaptoethanol) which was also used to equilibrate the column prior to the run. The fractions corresponding to the protein were pooled, concentrated to a final volume of ~1.5 mL and

the CjFur concentration was quantified by measurement of the A_{280} ($\epsilon_{280} = 0.646 \mu\text{L}/\mu\text{g}$, as determined with the ProtParam Tool from ExPASy) using a spectrophotometer (NanoDrop ND-1000, Thermo Scientific). To elicit the shift in conformation from the apo form to the holo form of CjFur, the protein sample was incubated with 3 molar equivalents of MnCl₂ overnight. Manganese has been reported to bind to Fur proteins and is often used as a cofactor for *in vitro* experiments, given that it is more stable than the natural coeffector of Fur proteins Fe²⁺ (Dubrac and Touati, 2002). MnCl₂ was added gradually to prevent protein precipitation which has been reported to occur during metal addition (Dian et al., 2011).

To remove the excess of manganese, the metallated holo-CjFur (or MnCjFur) was further purified through a second round of size-exclusion chromatography using the same gel filtration buffer, as described above. The appropriate fractions were subsequently pooled and concentrated to ~150 μL . Finally, the protein was dialyzed against 2L of EMSA binding buffer (20 mM Bis-Tris Borate pH 7.4, 50 mM KCl, 3 mM MgCl₂, 5% glycerol) during 1h at 4°C and re-quantified using the same method described before.

2.4. Screening of Crystallization Conditions for Apo-CjFur

The crystallization conditions for apo-CjFur were screened based on conditions that yielded positive results for the crystallization of another apo-CjFur construct. A custom-made crystallization kit (described in Appendix B: Crystallization of Apo-CjFur) was used in combination with the sitting-drop water diffusion method. Drops of 1 μL containing fresh protein (7.5 $\mu\text{g}/\mu\text{L}$) were combined in a 1:1 ratio with the mother liquors from the screening kit in the wells of a 96-well crystallization plate (Greiner) pre-filled with 70 μL of mother liquor in the reservoirs. Crystals grew over a period of 1 week in 0.1 M Bis-Tris pH 5.5, 0.25 M MgFormate, 25% PEG3350.

2.5. Initial X-Ray Diffraction Experiments for Apo-CjFur

Apo-CjFur crystals were harvested with a CryoLoop (Hampton Research) and soaked in the mother liquor supplemented with different cryoprotectants. The cryoprotectants used included MPD, glycerol, ethylene glycol and PEG400. The crystals were then flash-frozen in liquid nitrogen. The crystals were mounted on a HomeSource Micromax-007 X-Ray Diffraction System (Rigaku) and kept frozen in a nitrogen stream using a Cryostream Controller 700 (Oxford Cryosystems) set to 100 K. The crystals were exposed during 20 minutes to X-rays at a 1.54178 Å wavelength, and data was collected with a R-AXIS IV++ detector (Rigaku) at a 250 mm distance from the crystals.

2.6. Optimization of Crystallization Conditions for Apo-CjFur

The conditions that yielded the initial apo-CjFur crystals were used as a starting point for optimization of the previous crystallization experiments. Many conditions yielded large enough crystals exhibiting adequate morphologies for X-ray diffraction experiments. Optimal crystals were grown at 4°C in 0.1 M Bis-Tris pH 5.5, 0.25 M MgFormate, 21% PEG3350 over a period of 1 week.

2.7. Final X-Ray Diffraction Experiments for Apo-CjFur

The optimal CjFur crystals were harvested and cryoprotected in mother liquor supplemented with 7.5% glycerol prior to a complete data set collect using the method described in section 2.5. The dataset was integrated in HKL-2000 (HKL Research). The crystals were then

sent to the Argonne National Laboratory Advanced Photon Source (Chicago) to be exposed to X-rays from a synchrotron light source in order to generate a higher resolution data set.

2.8. Resolution of the Apo-CjFur Crystal Structure

An initial working model was built at the collect site using PHENIX (P. D. Adams et al., 2010). Phasing was done using molecular replacement using the apo-CjFur crystal structure deposited in the RCSB Protein Databank (PDB: 4ETS). The model was refined using the BUSTER software (Bricogne G. et al., 2011) and manual modifications to the model were done in Coot (Emsley et al., 2010). The quality of the model was assessed using Molprobity (Chen et al., 2010a) and RAMPAGE (Lovell et al., 2003).

2.9. Screening Crystallization Conditions for the Holo-CjFur-DNA Complex

In order to determine which DNA oligonucleotides would provide the crystals with the best diffraction qualities, a large set of crystallization experiments were performed. In total, 31 different oligonucleotides were screened within a wide range of conditions.

All oligonucleotides screened contained the CjFur binding site from the *katA* promoter region, which had been shown to associate with CjFur in previous electrophoretic mobility shift assays (EMSA) experiments performed in the laboratory (Butcher et al., 2012). The oligonucleotides screened varied in length (15-39 bp) and had different endings (blunt ends and cohesive ends). Previous studies have shown that the nature and length of the DNA oligonucleotides is crucial for crystallization, and that varying the sequence around a narrower set of conditions typically yields better results than screening a wide range of conditions around a narrow set of oligonucleotides (Pakotiprapha and Jeruzalmi, 2014). More details concerning the

oligonucleotides screened can be found in the Table 1 in Appendix C: Crystallization of the Holo-CjFur-DNA complex.

The commercially synthesized and purified single-stranded oligonucleotides (Eurofins MWG Operon) were resuspended in water to generate 1 mM stocks, which were quantified through measurement of their A₂₆₀. The single-stranded oligonucleotides were mixed with their complementary sequence to a final concentration of 400 µM in an annealing buffer (NEB2, New England Bioscience), melted during 10 minutes at 95°C to denature secondary structures, and let reach room temperature in a ramp during 2h to let the strands anneal gently. The annealed oligonucleotides were finally dialyzed in the EMSA binding buffer (described in section 2.3) during 1h.

The oligonucleotides were incubated on ice during 30 minutes with freshly purified holo-CjFur protein (2.5 µg/µL) in a 1.2 DNA: 1 holo-CjFur molar ratio to drive the association of the holo-CjFur-DNA complex and reduce species heterogeneity (liganded and unliganded protein) in the sample.

The crystallization experiments were performed at 4°C using the sitting drop vapour diffusion method described in section 2.4. A wide variety of commercial sparse matrix crystallization screening kits were used to screen for optimal crystallizations for the complex. A list of the kits used is provided in Appendix C: Crystallization of the Holo-CjFur-DNA complex.

2.10. Generation of the CjFur R14E and K17E Mutants

The CjFur R14E and K17E mutants were generated by site-directed mutagenesis using the QuickChange Site-Directed Mutagenesis Kit (Stratagene). The procedures recommended by the manufacturer were followed. The primers used and the PCR settings used can be found in

Appendix D: *In Vitro* Characterization of the CjFur R14E and K17E mutants. Plasmids were prepared using a mini-prep kit (BioBasic) according to the manufacturer's procedures. The mutant plasmids were sent for sequencing to the Plateforme de séquençage et de génotypage des génomes du CHUL (Québec City) in order to confirm that the desired mutations were introduced in the pStrep-CjFur construct.

2.11. *In Vitro* Characterization of the R14E and K17E Mutants

We sought to biochemically characterize the holo-CjFur mutants R14E and K17E through Electrophoretic Mobility Shift Assays (EMSA).

Both mutants were purified using the same purification protocol described in section 2.3.

A synthetic 60 bp Cy5-labeled DNA oligonucleotide (Eurofins MWG Operon) from the *katA* gene promoter region (1 nM) (see Appendix D: *In Vitro* Characterization of the CjFur R14E and K17E mutants) was incubated during 1h with increasing concentrations of the mutants (0-100 nM) in a EMSA binding buffer (20 mM Bis-Tris Borate pH 7.4, 50 mM KCl, 3 mM MgCl₂, 50 μM MnCl₂, 5% glycerol, 0.1% Triton X-100) previously determined to be optimal in EMSA experiments. 5 ng/μL poly(dI-dC) was used as a non-specific binding competitor. The samples were run during 1h at 100V and 4°C on a native 6% polyacrylamide gel supplemented with 100 mM Bis-Tris Borate pH 7.4, 100 μM MnCl₂ that had been pre-run during 25 minutes at 150V. All the steps were carried out in the dark to limit the exposure of the Cy5 fluorophores to light, which results in decreased fluorescence signals.

The gels were imaged with a Typhoon Trio Variable Mode phosphoimager (GE Healthcare) and processed in ImageJ (Abràmoff et al., 2004) to improve the brightness and contrast of the images.

The apparent dissociation constants (K_d) of the mutant-DNA complexes were calculated using the one-site ligand binding curve of GraphPad Prism (GraphPad Software). The experiment was performed in triplicate to allow for the calculation of standard deviation values.

3. Results

3.1. Purification of CjFur WT

The majority of crystallization experiments require large quantities of highly pure protein (Rhodes, 2006). To purify large quantity of proteins, one must first find the appropriate host for protein overexpression and find the optimal overexpression conditions. *E. coli* has been determined to be an appropriate overexpression system for CjFur which is a prokaryotic protein with no major post-translational modifications. It is practical, cheap and allows for high protein yields.

The protein was successfully overexpressed in *E. coli* BL21 Rosetta cells optimized for overexpression of recombinant proteins, as can be seen from the protein content of the crude lysate. An intense band corresponding to the tagged CjFur monomer with a calculated molecular mass of ~21.1 kDa is seen on a SDS-PAGE gel (Figure 4A). Clarification of the crude extract shows that the protein is soluble in the buffer used for protein extraction, as no significant loss in band intensity can be detected after the removal of insoluble components by high-speed centrifugation (soluble extract).

Affinity chromatography on Strep-Tactin resin drastically increases protein purity, although some contaminants co-elute with CjFur. Non-specific binding of contaminants to the resin cannot be excluded. The shift in the mobility of the band observed following Strep-Tag cleavage step suggests that most of the protein is in the untagged form following cleavage, although more sensitive methods such as mass spectrometry would be required to confirm it. This step is vital, as protein tags can interfere with a protein's structure and function (Malhotra, 2009).

On the size-exclusion chromatogram (Figure 4B), CjFur elutes slightly before the 44 kDa marker, which corresponds to a higher molecular mass than that of the CjFur dimer. The fractions

collected from the size-exclusion chromatography steps however confirm that the protein eluted from the column runs to ~18 kDa on an SDS-PAGE gel (Figure 4A). This suggests that the protein purified by size-exclusion chromatography corresponds to CjFur. The protein seemingly co-elutes from the size-exclusion chromatography (both runs) alongside a contaminant which runs to ~36 kDa on an SDS-PAGE gel. Oddly, this corresponds to the molecular mass of the CjFur dimer. Worthy of mention is the fact that, in all cases, CjFur is found in higher proportions than the contaminant, as can be inferred from the intensity of the bands.

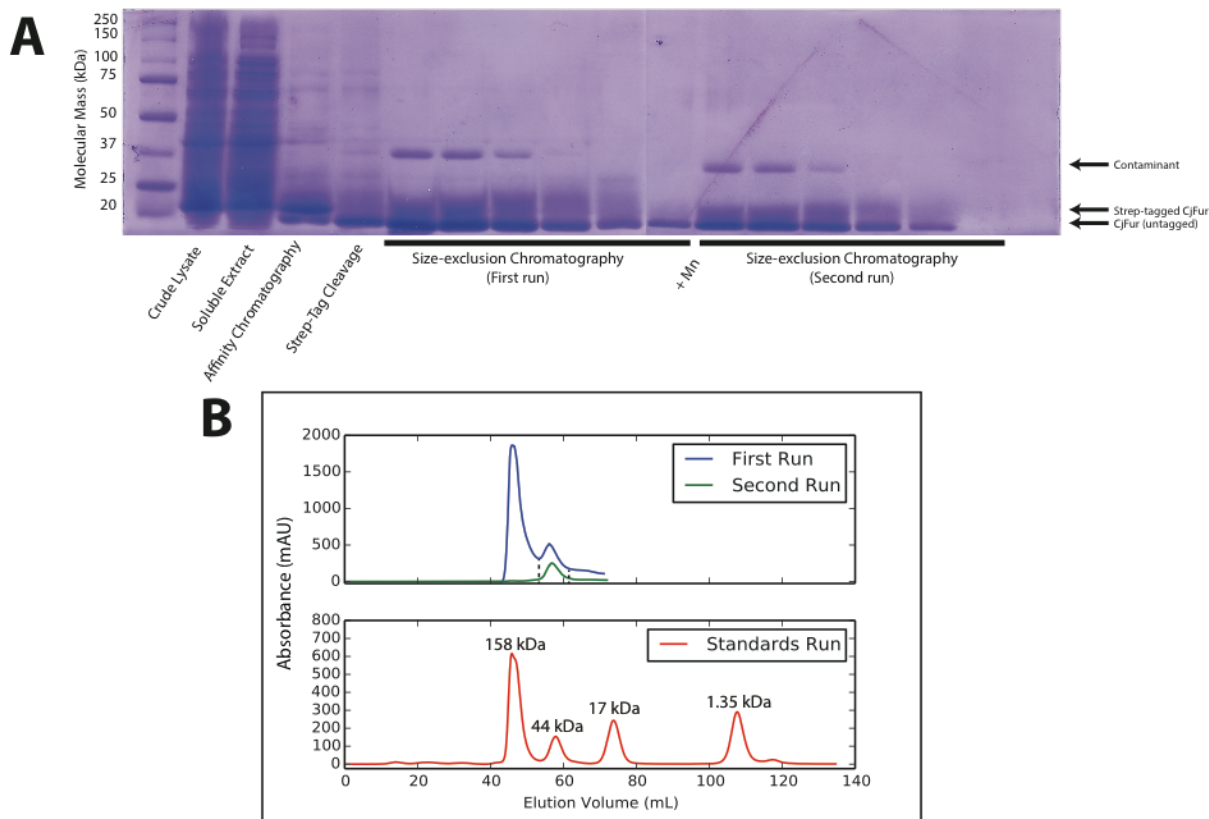


Figure 4. Purification of CjFur WT

(A) *E. coli* BL21 Rosetta competent cells (Novagen) expressing the pStrep-CjFur WT were lysed by sonication on ice. The lysate was clarified by high-speed centrifugation. CjFur was purified using affinity chromatography on Strep-Tactin resin (Qiagen) and the Strep-Tag was cleaved during 16 hours. The CjFur was further purified using size-exclusion chromatography on a Superdex75 (GE Healthcare). The protein was metallated with 3 molar equivalents Mn and incubated overnight. Finally, the protein underwent another run of size-exclusion chromatography in the same column. 5 µL samples were separated on a 12% SDS-PAGE gel to assess protein purity. **(B)** The size-exclusion chromatograms of CjFur WT are shown. The top panel shows the curves corresponding to the first run (blue) and the second run (green). The dashed vertical lines correspond to the outermost fractions collected. The bottom panel shows the elution profile of molecular weight markers (red). The marker peaks are labeled according to their molecular weight.

3.2. Crystallization of Apo-CjFur

To obtain diffraction quality crystals, we carried out various crystallization screenings (Figure 5A). Following several optimization steps, crystals exhibiting birefringent properties and regular 3D morphologies were obtained. The crystals grew in the shape of a screwdriver head.

Imperfections in a crystal result in a decrease in the quality of the diffraction data. Defects may increase mosaicity, or the irregularity of reflection planes in a crystal (Dobrianov et al., 1999). The regularity of these reflection planes in the crystal is key in generating the interferences of X-rays required by X-ray crystallography. The faces of the apo-CjFur crystals were smooth and regular and bore no obvious bulk defects such as cracks, voids, impurity clusters or twins, making them good candidates for X-ray diffraction experiments.

The diffraction pattern generated using a MicroMax 007HF (Figure 5B) showed that the optimal crystal diffracts X-rays to a resolution of at least 2.1 Å. A 2.1 Å resolution is sufficient to show the precise location of the amino acids within the protein structure (Rhodes, 2006).

The diffraction pattern generated at the Synchrotron Light Source improved the resolution to a final value of 1.8 Å (data not shown).

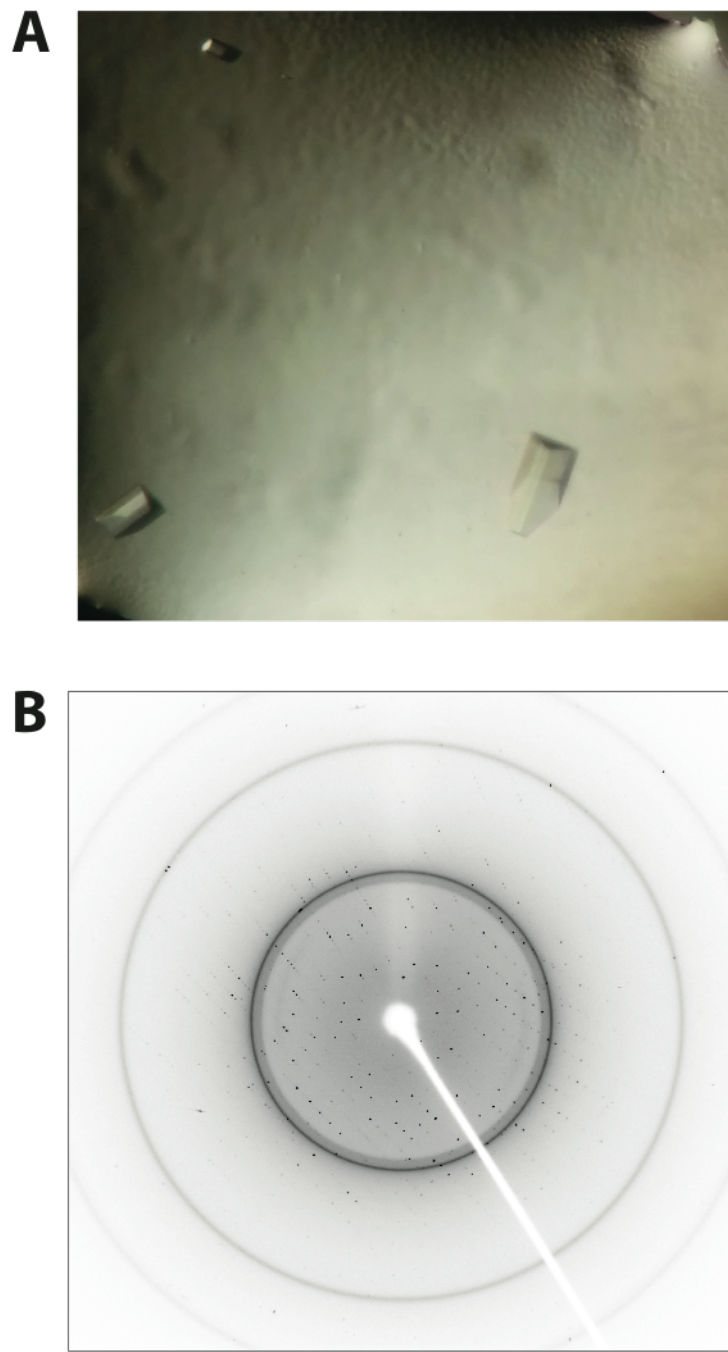


Figure 5. Crystals and diffraction pattern of the new apo-CjFur construct

(A) Crystals of apo-CjFur were grown over a 1 week period at 4°C using the sitting drop water diffusion method in 0.1 M Bis-Tris pH 5.5, 0.25 M MgFormate and 21% PEG3350. **(B)** Representative diffraction pattern obtained from a crystal harvested, cryoprotected in 7.5% glycerol and flash-frozen in liquid nitrogen.

3.3. Crystal Structure of Apo-CjFur

The crystal structure of the new apo-CjFur protein construct was built and refined to a final $R_{\text{work}}/R_{\text{free}}$ ratio of 0.2346/0.2712 at a 1.8 Å resolution (Figure 6A). The bond lengths in the model have a root mean square deviation (RMSD) value of 0.01 Å, while angles have an RMSD value of 1.05°. The Ramachandran plot was used to evaluate the validity of the protein model, based on the Φ and Ψ angles in the protein main chain (Voet and Voet, 2011). Analysis of the angles in the new apo-CjFur model revealed that the vast majority these angles fell within favored and allowed regions (98.9% favored, 0.8% allowed) of the Ramachandran plot (Figure 7). Only Lys97 in one of the monomers was modeled with bond angles unallowed by Ramachandran's rules and steric repulsion constraints.

The model shows that the protein assembles into a biological dimer (Figure 6B). Each monomer folds in two domains, the DBD and the DD, reminiscent of other ferric uptake regulators. The DBD contains 5 α -helices ($\alpha_1, \alpha_2, \alpha_3, \alpha_{3-2}, \alpha_4$) and β -strands β_1 and β_2 . The DD contains three β -strands ($\beta_3-\beta_5$) followed by one α -helix (α_5). Close inspection of the DBD reveals that the α_1 -helix is oriented towards the inside of the V-cleft. The electrostatic surface potential contour map generated from the crystal structure (Figure 6C) shows that the DBD has a largely positively charged surface, especially the surface at the extremity of the DBD facing away from the cleft. The surface at the bottom of the V-cleft has a globally negative charge.

The CjFur adopts the V-shaped conformation seen in the crystal structural of the previous apo-CjFur construct (Figure 6B).

One of the two metal atoms characterized in the previous apo-CjFur structure could be detected in the new apo-CjFur monomers (Figure 8). This metal, which is most likely zinc, corresponds to the structural zinc tetra-coordinated by Cys105, Cys108, Cys145 and Cys148 in

the S1 metal binding site. The length of all four coordination bonds is 2.3 Å (not shown), a value consistent with measurements of the S1 site in other metalloregulators.

A

| Apo-CjFur WT | |
|-----------------------------|---|
| Data collection | |
| Space group | P2 ₁ 2 ₁ 2 ₁ |
| Geometry | Orthorombic |
| Cell dimensions | |
| a, b, c (Å) | 35.713, 84.410, 123.678 |
| α, β, γ (°) | 90, 90, 90 |
| Resolution (Å) | 1.81-69.72 |
| Completeness (%) | 99.88 |
| Refinement | |
| No. reflections | 34 996 |
| R _{work} | 0.2346 |
| R _{free} | 0.2712 |
| B-factors (Å ²) | |
| Average | 25.18 |
| RMSD | |
| Bond lengths (Å) | 0.01 |
| Bond angles (°) | 1.05 |

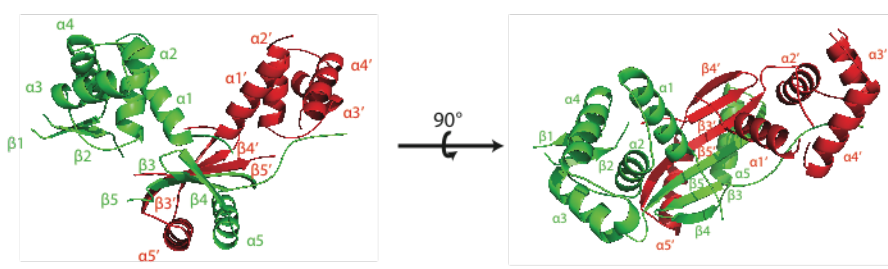
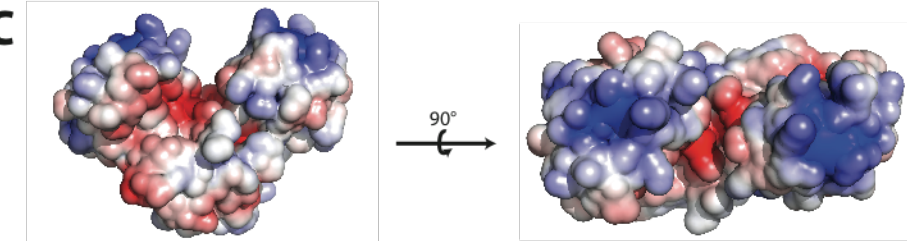
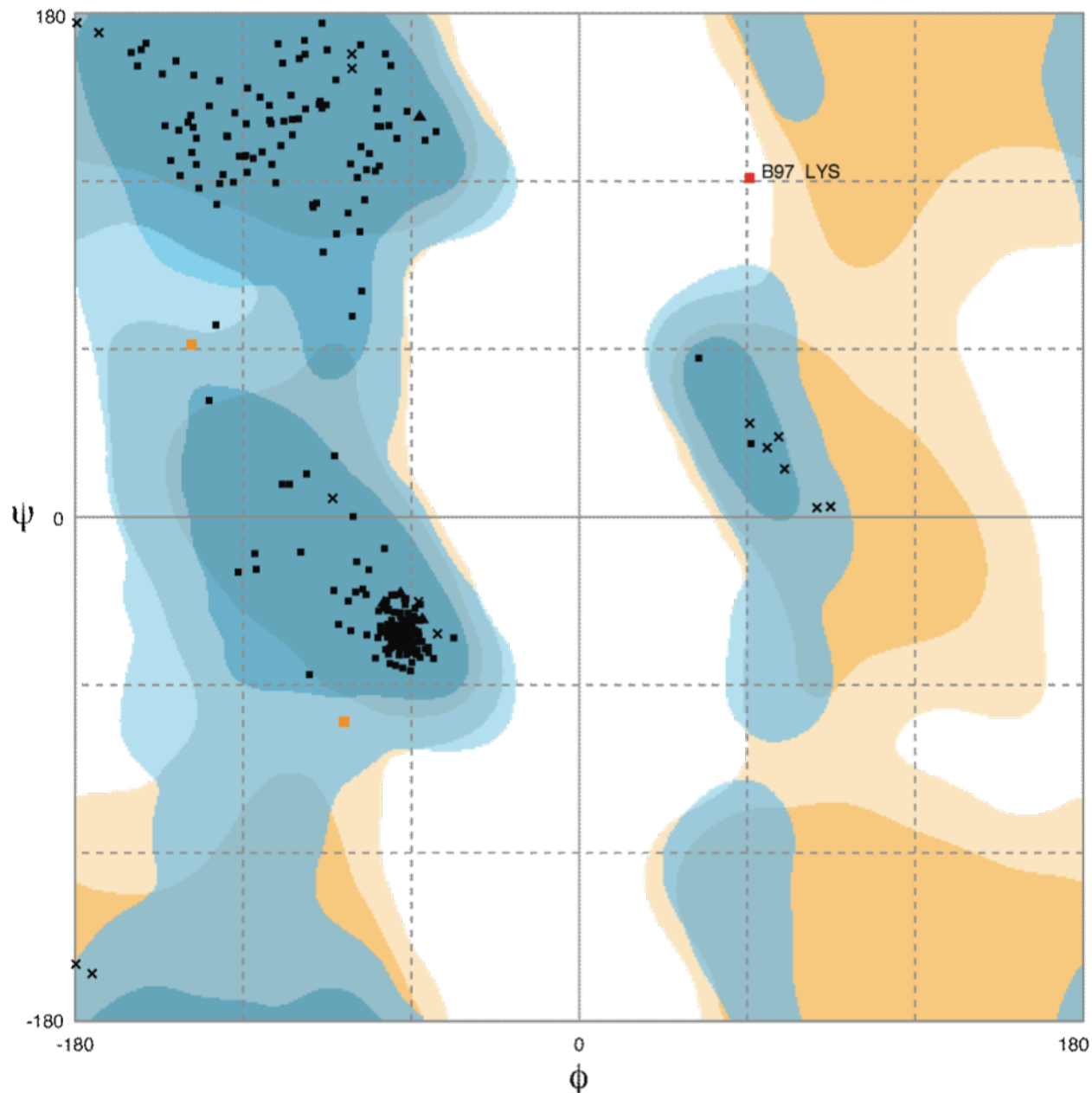
B**C**

Figure 6. Crystal Structure of the new apo-CjFur construct

(A) Relevant model statistics for the new crystal structure of apo-CjFur crystallized from the pStrep-CjFur WT construct are listed in a table. (B) The crystal structure of apo-CjFur was built and refined with Coot (Emsley et al., 2010) and BUSTER (Bricogne et al., 2011), respectively. The crystal structure shown was rendered in PyMol (Schrodinger). The monomers are shown in red and green. Secondary structures are labeled. (Structural metal atoms are not shown.) (C) The electrostatic surface potential of the newly obtained crystal structure of apo-CjFur was generated with the PDB2PQR (Dolinsky et al., 2004) and APBS (Baker et al., 2001) plugins in PyMol. The electrostatic potential is contoured from -5 k_bT⁻¹ to 5 k_bT⁻¹ (k_b: Boltzmann's constant, T: temperature, e: charge of an electron). Positively charged regions are in blue, whereas negatively charged regions are in red.



| | | | |
|---|----------------------------------|---|---------------------------------|
| ■ ▲ | General/Pre-Pro/Proline Favoured | ■ ▲ | General/Pre-Pro/Proline Allowed |
| × | Glycine Favoured | × | Glycine Allowed |

Number of residues in favoured region (~98.0% expected) : 258 (98.9%)

Number of residues in allowed region (~2.0% expected) : 2 (0.8%)

Number of residues in outlier region : 1 (0.4%)

Figure 7. Ramachandran plot of the new apo-CjFur model

The Ramachandran plot of the new apo-CjFur model was generated using the online tool RAMPAGE (Lovell et al., 2002).

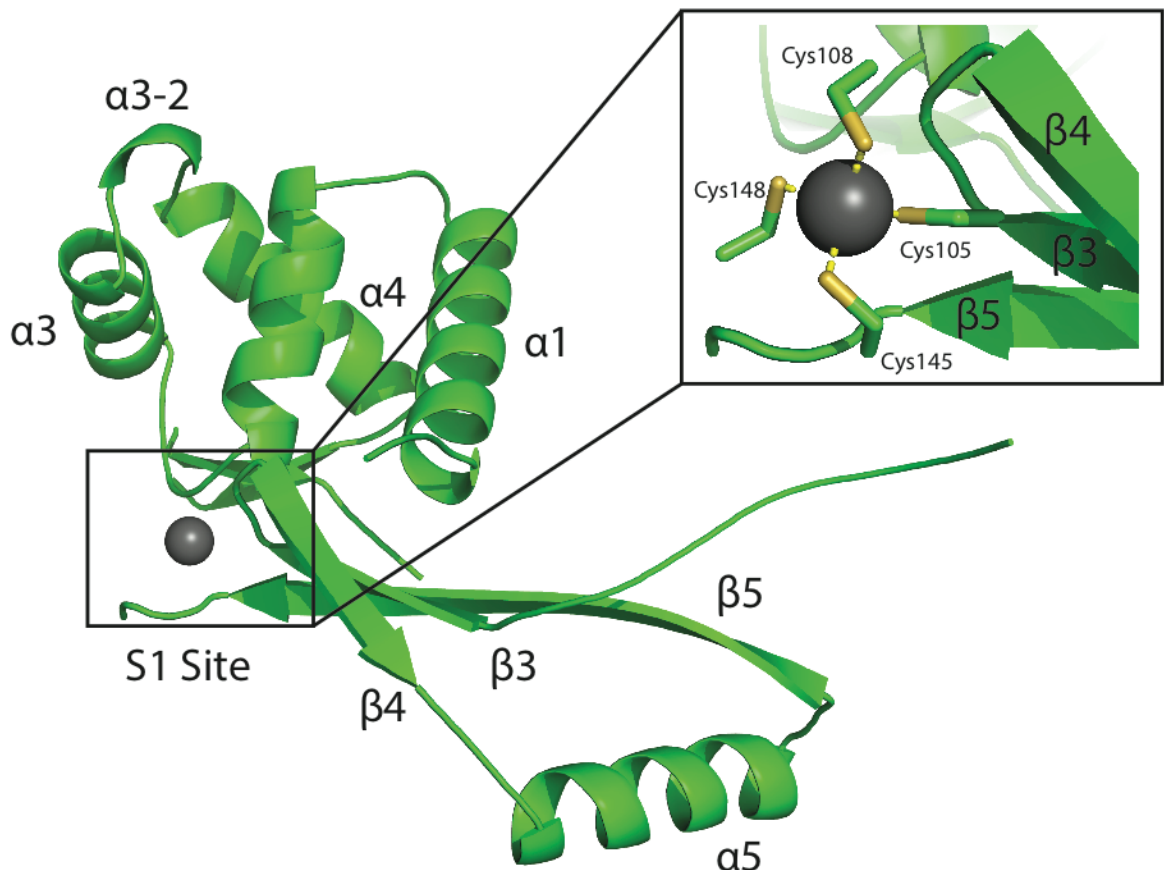


Figure 8. The S1 metal binding site in the new apo-CjFur crystal structure

The S1 metal binding site of apo-CjFur was rendered in PyMol. Shown are the location of the S1 metal binding site within the structure of a CjFur monomer and an enlarged view of the details and geometry of the metal binding site, which tetra-coordinates a metal atom.

3.4. Comparative analysis of the apo-CjFur structures obtained with different tagging strategies

The two crystal structures of apo-CjFur were compared. The first apo-CjFur crystal structure comprises four extraneous residues in N-terminus. These residues, which engage in strong interactions with the DD of apo-CjFur, are remnants of the SUMO tag that was used to purify the protein. The new apo-CjFur crystal structure purified using a different protein construct was designed such that the final protein product is the native CjFur WT protein with only one additional Gly residue in N-terminal. Due to its small size and hydrophobic nature, the Gly residue is unlikely to engage in strong interactions with the dimerization domain of apo-CjFur.

All residues present in the new crystal structure belong to the CjFur native amino acid sequence, as the electron density map failed to show electron density for the extra glycine residue that remains appended to the wild-type protein after the tag cleavage step. This result provides, together with our SDS-PAGE analysis, further evidence that the tag was cleaved off the protein construct.

Our results show that both crystal structures obtained using a construct align well. A structural alignment of a monomer from each structure showed that they both assume the same overall conformation (Figure 9). The secondary structures in both models superpose well and adopt the same orientations. The position and conformation of the DBD with respect to the DD position is virtually identical in both structures with an overall RMSD of 1.651 Å.

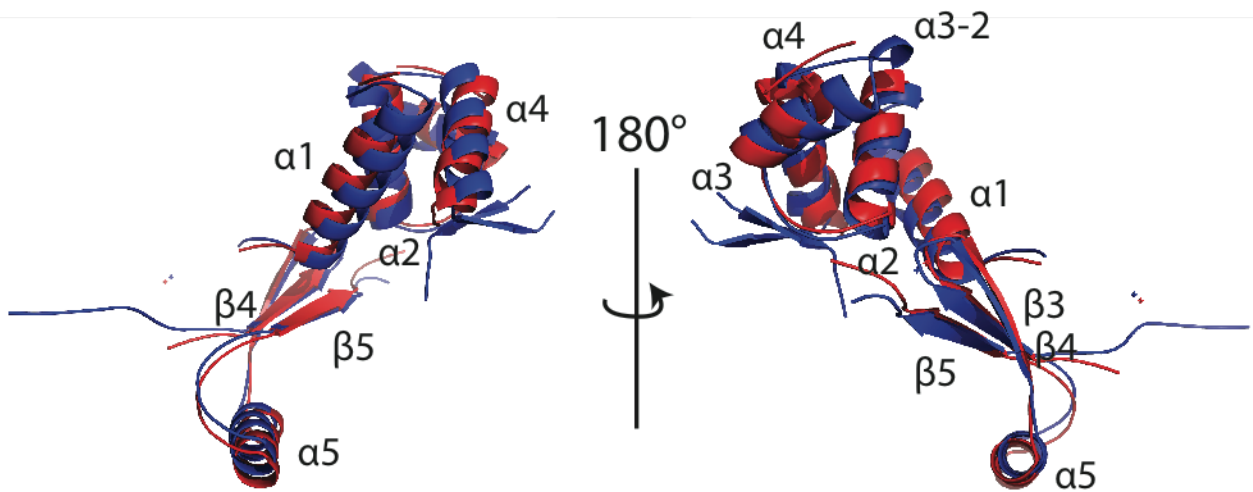


Figure 9. Structural alignment of the old and new CjFur crystal structures

Monomers from the old and new crystal structures of apo-CjFur were superposed and rendered in PyMol. The first apo-CjFur structure is in red, whereas the new one is shown in blue. 180° rotations of the same alignment are shown.

3.5. Crystallization of the Holo-CjFur-DNA Complex

Important efforts have been invested in trying to crystallize the holo form of CjFur in complex with one of its DNA targets. Success in doing so would not only show how the protein interacts with DNA in presence of iron and what structural features are involved in holo-CjFur's specificity for its DNA targets. It would also reveal the structural changes undergone by CjFur upon binding iron and provide additional evidence for the holo-regulation mode and its putative structural basis.

A wide variety of DNA oligonucleotides have been screened in order to grow diffraction-quality crystals of the holo-CjFur-DNA complex. Crystals were grown successfully in a narrow range of conditions. However, none of them reached a sufficient size or displayed morphological features necessary for X-ray diffraction data collection.

In general, shorter DNA oligonucleotides (<30 bp) yielded better results than longer ones, which mostly failed to lead to crystal formation. The nature of the oligonucleotide ends (cohesive or blunt), however, did not seem to change the potential of a complex to form crystals for the oligonucleotides tested.

The crystals grown took the shape of needles, coffee beans, or had hair-like protuberances (Figure 10A-C). One particular condition yielded small crystals that had an octahedron-like shape (Figure 10D). Although small, the crystals were subjected to an X-ray diffraction experiment, which showed that the crystals were probably DNA crystals, as they generated a diffraction pattern characteristic of DNA molecules (Figure 10E). It is unclear whether the protein co-crystallized with the DNA given the low resolution of the diffraction pattern and the limited quantity of reflections measured.

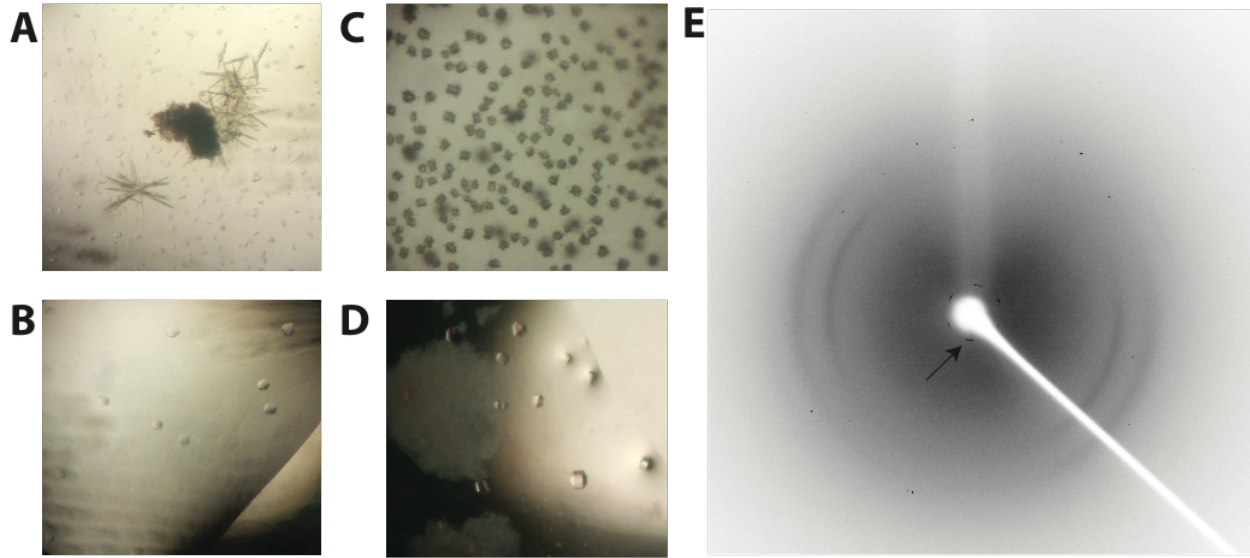


Figure 10. Crystals obtained following crystallization screenings with the holo-CjFur-DNA complex

Shown are typical results obtained during crystallization experiments of the holo-CjFur-DNA complex. The DNA oligonucleotides sequences are shown in Appendix C: Crystallization of the Holo-CjFur-DNA complex. **(A)** Needle shaped crystals sharing a same nucleation center were grown in 0.1 M Bis-Tris pH 5.5, 17% PEG4000, 0.25 M MgCl₂ with a 20 bp DNA oligonucleotide (JFC2390-91). **(B)** Coffee bean shaped crystals were grown in 0.1 M Bis-Tris pH 7.0, 15% PEG4000, 0.25 M MgAc with a 20 bp DNA oligonucleotide (JFC2390-91). **(C)** Crystals with hair-like protuberances were grown in 0.1 M Bis-Tris pH 5.5, 21% PEG3350, 0.25 M MgFormate with a 25 bp DNA oligonucleotide (JFC2400-01). **(D)** Crystals showing an octahedron-like shape were grown in 0.1 M Bis-Tris pH 5.4, 25% PEG3350, 0.1 M MgCl₂ with a 25 bp DNA oligonucleotide (JFC2400-01). **(E)** The crystals shown in (D) were cryoprotected in 15% ethylene glycol, flash-frozen in liquid nitrogen, and exposed to X-rays for 20 mins. An arrow points to the reflections characteristic of DNA diffraction patterns.

3.6. *In Vitro* Characterization of the CjFur R14E and K17E Mutants

Many residues in the CjFur DBD have been characterized *in vitro* using mutational studies and electrophoretic mobility shift assays (EMSA) to assess their involvement in the DNA binding activity of the protein in apo and holo conditions. Residues R14 and K17 are located within the α 1-helix of the CjFur DBD, near the V-cleft, but oriented outwards, making them unlikely to engage in interactions with DNA. Their involvement in the DNA binding activity of CjFur has been characterized under apo conditions. Mutating R14 and K17 to Glu residues did not impair DNA binding by apo-CjFur (data not published).

Additional electrophoretic mobility shift assays (EMSA) were performed to determine whether residues R14 and K17 are reoriented in way that permits interactions between the residues and DNA in holo-CjFur.

The EMSA results show that both mutants retain their ability to bind to DNA as demonstrated by the shift in the Cy5 labeled oligonucleotide probe mobility (Figure 11B). Interestingly, multiple species exist for the bound probe. Curiously, the K17E mutant shifts DNA more abruptly to higher molecular mass species than the R14E mutant and the wild-type protein.

The calculated apparent dissociation constants (K_d) are similar for both mutants and the wild-type protein. A K_d of 2.14 ± 0.25 nM was determined for holo-CjFur WT (data not shown), whereas values of 1.99 ± 0.39 nM and 3.60 ± 0.87 nM were calculated for the R14E and K17E mutants, respectively. These results provide quantitative evidence against the involvement of R14 and K17 in the DNA binding activity of holo-CjFur in the conditions tested.

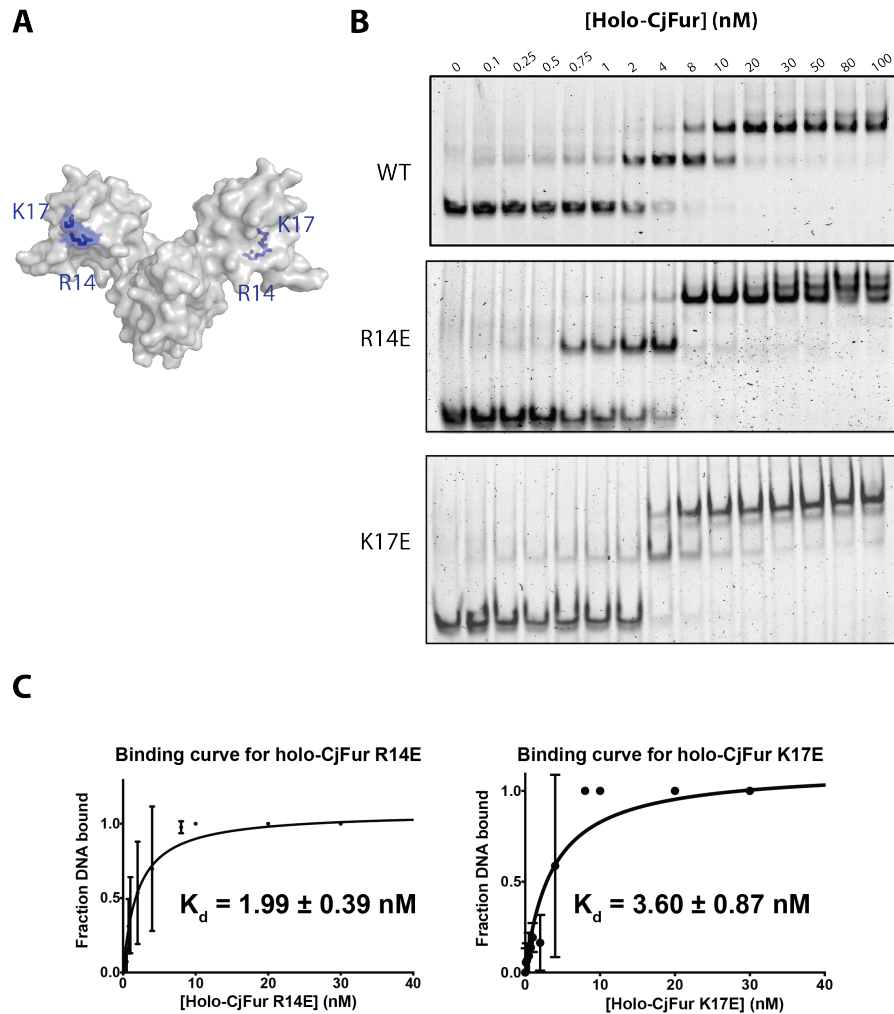


Figure 11. Characterization of the holo-CjFur R14E and K17E mutants by EMSA

(A) The structure of holo-CjFur was modeled in PyMol based on the homology between CjFur and HpFur. The CjFur DBD was rotated so that it aligns with the DBD of holo-HpFur (PDB: 2XIG). The residues highlighted in blue were mutated to Glu to evaluate their role in the DNA binding activity of holo-CjFur with DNA. (B) A Cy5 labeled probe corresponding to a 60 bp fragment from the *katA* gene promoter region (1 nM) was titrated with increasing concentrations (0-100 nM) of holo-CjFur WT (top), R14E (middle) and K17E (bottom) and run on a native polyacrylamide gel. The experiment was performed in triplicate. (C) The strength of holo-CjFur-DNA association for the R14E and K17E mutants was quantified using ImageJ for densitometry analysis and GraphPad Prism (GraphPad) for apparent K_d determination using non-linear data regression. The data was fit to the equation for one-site specific ligand binding: $Y = B_{\max} * X / (K_d + X)$ (Y : fraction bound, B_{\max} : maximum specific binding, K_d : apparent dissociation constant, X : ligand concentration). Mean apparent K_d values are given \pm their standard deviation.

4. Discussion

We sought to validate two concepts through our studies. First, we looked to confirm the hypothesis that the SUMO tag remnants present in previously published apo-CjFur structure do not “lock” the apo-CjFur DBD into its atypical orientation using a different tagging approach. Second, we were interested in gathering additional data to support our model, which provides a structural basis for the different regulation modes of CjFur. In our model, the binding of an iron atom in the metal binding site S2 triggers a conformational change in the flexible hinge region of CjFur. We believe that it results in the rotation of the DBD and, ultimately, in the shift from apo regulation to holo regulation as well as in a change in the affinity of CjFur for different DNA binding motifs.

We were successful in purifying apo-CjFur WT to a level of purity sufficient for crystallographic studies. CjFur WT seems to co-elute along with a still unidentified contaminant. It is reasonable to suspect that this contaminant corresponds to the CjFur dimer for two reasons. First and foremost, the contaminant migrates to the dimer molecular mass mark on an SDS-PAGE gel. Second, our subsequent experiments have shown that the protein could be crystallized in these conditions. It is a well-established fact that protein heterogeneity in a sample can interfere with its ability to crystallize (Rhodes, 2006). It is unclear, however, why CjFur could retain its dimer conformation following denaturation in β -mercaptoethanol and SDS. The precise identity of the contaminant could be determined by protein sequencing using tandem mass spectrometry or Edman degradation.

Our experiments allowed us to crystallize and solve the crystal structure of a new CjFur construct. The R/R_{free} ratio, which measures the agreement between the model and the diffraction data, was determined to be 0.2346/0.2712, suggesting that there is an acceptable fit between the

model and the experimental data and that the data was not overmodelled (Rhodes, 2006). Analysis of bond angles and lengths support the validity of our new model, as demonstrated through Ramachandran analysis of the Φ and Ψ bond angles and calculation of RMSD values which are all within the accepted range (Rhodes, 2006). Overall, these observations show that our new model was refined to a degree sufficient for comparison with the previously solved apo-CjFur structure.

Failure to detect other metals than the one tetracoordinated in the S1 metal binding site in the electron density map provides a first indication that the CjFur structure solved is in the apo form. It also raises a question in regards to the nature of the S3 metal binding site previously shown to coordinate a zinc atom (Butcher et al., 2012). The absence of electron density in the S3 site could be caused by a high B-factor (lack of a precise position within the molecules in the crystal), which would explain its decreased ability to diffract X-rays and its capacity to evade detection (Rhodes, 2006). The presence of zinc in the S3 site could be precisely determined by inductively coupled plasma mass spectrometry (ICP-MS) (Butcher et al., 2012). In the event that ICP-MS failed to show the presence of a second zinc atom within the S3 site, we would be prompted to characterize the S3 site through mutational studies to see whether it contributes to the proper folding of CjFur, which is the current belief (Butcher et al., 2012). The essentiality of these “structural sites” is still matter to discussions as there are contradicting reports among Fur homologs (Dian et al., 2011; Fillat, 2014; Lee and Helmann, 2007; Lewin et al., 2002; Sheikh and Taylor, 2009).

Structural alignment of the two apo-CjFur models reveals that the two proteins align with an RMSD of 1.651 Å suggesting that both structures are similar (Carugo and Pongor, 2001). Slight differences in the positions of certain secondary structures such as the α 1- α 4 within the models could be accounted for by the divergence in the crystal packing of the protein. These results strongly demonstrate that the SUMO tag remnants, which are absent in the new crystal structure

of apo-CjFur, were not responsible for the peculiar orientation adopted by the DBD of CjFur and further support the the model wherein CjFur DBD adopts different conformations to accommodate apo and holo regulation, as seen in *C. jejuni* and *H. pylori* (Butcher and Stintzi, 2013; Butcher et al., 2012; Dian et al., 2011; Fillat, 2014).

Attempts to generate diffraction quality crystals of the holo-CjFur-DNA complex were unsuccessful. Short DNA oligonucleotides seemed to generate better results than longer ones in general. This is consistent with the literature, which suggests trying to start crystallization experiments with smaller oligonucleotides and to increase their length gradually (Pakotiprapha and Jeruzalmi, 2014). Some explanations could rationalize our difficulties in crystallizing holo-CjFur-DNA complex. First, our preliminary studies have shown that apo-CjFur may be more stable than holo-CjFur and more apt to form crystals in the wild-type form of the protein. Our attempts to generate holo-CjFur crystals yielded apo-CjFur crystals (data not shown). This may contribute to the difficulties faced while trying to crystallize the protein with a DNA oligonucleotide containing the holo-CjFur binding motif. Interactions with DNA could potentially stabilize holo-CjFur, but there is insufficient data to confirm this hypothesis. Second, EMSA experiments have shown that holo-CjFur oligomerizes to varying degrees when binding to DNA (Butcher et al., 2012). This increased heterogeneity may interfere with the crystal growth. The problem could be tackled from different angles. EcZur was co-crystallized with a DNA target for which it has a very high affinity with an apparent dissociation constant in the attomolar range (Gilston et al., 2014). The affinity of holo-CjFur for the probe used in the EMSA experiments is much weaker with an apparent dissociation constant of roughly 2 nM (data not published). Finding a DNA target to which holo-CjFur binds with a higher affinity may increase the likelihood of crystallizing the holo-CjFur-DNA complex. Sequential Evolution of Ligands by Exponential Enrichment (SELEX)

could help identify the DNA motifs to which holo-CjFur binds with the highest affinity (Ogawa and Biggin, 2012). Crystallization may be facilitated, as associating the holo-CjFur-DNA complex using a higher affinity target would reduce heterogeneity in the sample and increase the fraction of DNA-bound holo-CjFur. Another approach would consist in stabilizing the holo-CjFur conformation of the protein through mutational surface engineering (Derewenda, 2004; Derewenda and Vekilov, 2006). In this technique, bulky charged residues Glu and Lys are mutated to residues with lower intrinsic entropy (alanine being the most commonly used) in order to decrease the entropic cost associated with the formation of a highly ordered crystal. This technique was previously used to improve crystal formation and diffraction of proteins refractory to crystallization (Derewenda et al., 2004; Longenecker et al., 2001; Munshi et al., 2003).

Our EMSA experiments show that R14 and K17 are not involved in the DNA binding activity of holo-CjFur in the experimental conditions tested. This is in line with our model in which holo-CjFur rotates its DBD upon iron binding in the S2 metal binding site, as R14 and K17 in our hypothetical model are oriented in a position that makes them unlikely to engage in intermolecular interactions with DNA. Our data also shows that holo-CjFur forms at least 2 oligomer species bound to DNA in the R14E and K17E holo-CjFur mutants. Interestingly, the K17E mutant seems to form little of the intermediate species and to shift more abruptly towards the larger oligomeric forms. This raises the possibility that the K17E holo-CjFur mutant binds cooperatively to its DNA target and that K17 may somehow prevent cooperative binding in holo-CjFur WT. The structural basis underlying cooperative binding of EcZur has been elucidated. EcZur's cooperative binding to DNA is mediated by the formation across the DNA helix of salt bridges between dimers (Gilston et al., 2014). Further work would be needed to better understand if and how K17 influences the cooperativity of the holo-CjFur's binding to DNA.

In conclusion, this study provides further evidence towards the existence of apo-CjFur and apo regulation in *C. jejuni*. We also show that R14 and K17 are not involved in the DNA binding activity of holo-CjFur under the conditions tested. These results support our hypothetical model describing the structural basis for holo regulation by CjFur, and the importance of the DBD of CjFur in modulating the CjFur regulation mode. Overall, our work provides additional structural data on CjFur, data which may find applications in drug discovery and design.

5. References

- Abergel, R.J., Zawadzka, A.M., Hoette, T.M., and Raymond, K.N. (2009). Enzymatic hydrolysis of trilactone siderophores: where chiral recognition occurs in enterobactin and bacillibactin iron transport. *J. Am. Chem. Soc.* *131*, 12682–12692.
- Abràmoff, M.D., Magalhães, P.J., and Ram, S.J. (2004). Image processing with imageJ. *Biophotonics Int.* *11*, 36–41.
- Andrews, S.C., Robinson, A.K., and Rodríguez-Quiñones, F. (2003). Bacterial iron homeostasis. *FEMS Microbiol. Rev.* *27*, 215–237.
- Bagg, A., and Neilands, J.B. (1987). Ferric uptake regulation protein acts as a repressor, employing iron(II) as a cofactor to bind the operator of an iron transport operon in *Escherichia coli*. *Biochemistry* *26*, 5471–5477.
- Baker, N. a, Sept, D., Joseph, S., Holst, M.J., and McCammon, J. a (2001). Electrostatics of nanosystems: application to microtubules and the ribosome. *Proc. Natl. Acad. Sci. U. S. A.* *98*, 10037–10041.
- Batz, M.B., Hoffmann, S., and Morris J. Glenn, J. (2012). Ranking the Disease Burden of 14 Pathogens in Food Sources in the United States Using Attribution Data from Outbreak Investigations and Expert Elicitation. *J. Food Prot.* *75*, 1278–1291.
- Braun, V. (2001). Iron uptake mechanisms and their regulation in pathogenic bacteria. *Int. J. Med. Microbiol.* *291*, 67–79.
- Bricogne, G., Blanc, E., Brandl, M., Flensburg, C., Keller, P., Paciorek, W., Roversi, P., Sharff, A., Smart, O.S., Vonrhein, C., et al. (2011). BUSTER version 2.10.1.
- Butcher, J., and Stintzi, A. (2013). The transcriptional landscape of *Campylobacter jejuni* under iron replete and iron limited growth conditions. *PLoS One* *8*, e79475.
- Butcher, J., Flint, A., Stahl, M., and Stintzi, A. (2010). *Campylobacter Fur and PerR Regulons. In Iron Uptake and Homeostasis in Microorganisms*, S.C.A. Pierre Cornelis, ed. (Norfolk, UK: Caister Academic Press), pp. 167–202.
- Butcher, J., Sarvan, S., Brunzelle, J.S., Couture, J.-F., and Stintzi, a. (2012). Structure and regulon of *Campylobacter jejuni* ferric uptake regulator Fur define apo-Fur regulation. *Proc. Natl. Acad. Sci.* *109*, 10047–10052.
- Carugo, O., and Pongor, S. (2001). A normalized root-mean-square distance for comparing protein three-dimensional structures. *Protein Sci.* *10*, 1470–1473.

- Chen, V.B., Arendall, W.B., Headd, J.J., Keedy, D. a., Immormino, R.M., Kapral, G.J., Murray, L.W., Richardson, J.S., and Richardson, D.C. (2010a). MolProbity: All-atom structure validation for macromolecular crystallography. *Acta Crystallogr. Sect. D Biol. Crystallogr.* *66*, 12–21.
- Chen, X., Naren, G.-W., Wu, C.-M., Wang, Y., Dai, L., Xia, L.-N., Luo, P.-J., Zhang, Q., and Shen, J.-Z. (2010b). Prevalence and antimicrobial resistance of *Campylobacter* isolates in broilers from China. *Vet. Microbiol.* *144*, 133–139.
- Dash, S., R Pai, A., Kamath, U., and Rao, P. (2014). Pathophysiology and diagnosis of Guillain-Barré syndrome -challenges and needs. *Int. J. Neurosci.* *2014 May 2*, [Epub ahead of print].
- Derewenda, Z.S. (2004). Rational protein crystallization by mutational surface engineering. *Structure* *12*, 529–535.
- Derewenda, Z.S., and Vekilov, P.G. (2006). Entropy and surface engineering in protein crystallization. *Acta Crystallogr. Sect. D Biol. Crystallogr.* *62*, 116–124.
- Derewenda, U., Mateja, A., Devedjiev, Y., Routzahn, K.M., Evdokimov, A.G., Derewenda, Z.S., and Waugh, D.S. (2004). The structure of *Yersinia pestis* V-antigen, an essential virulence factor and mediator of immunity against plague. *Structure* *12*, 301–306.
- Dian, C., Vitale, S., Leonard, G. a., Bahlawane, C., Fauquant, C., Leduc, D., Muller, C., De Reuse, H., Michaud-Soret, I., and Terradot, L. (2011). The structure of the *Helicobacter pylori* ferric uptake regulator Fur reveals three functional metal binding sites. *Mol. Microbiol.* *79*, 1260–1275.
- Dobrianov, I., Caylor, C., Lemay, S.. G., Finkelstein, K.. D., and Thorne, R.. E. (1999). X-ray diffraction studies of protein crystal disorder. *J. Cryst. Growth* *196*, 511–523.
- Dolinsky, T.J., Nielsen, J.E., McCammon, J.A., and Baker, N. a. (2004). PDB2PQR: An automated pipeline for the setup of Poisson-Boltzmann electrostatics calculations. *Nucleic Acids Res.* *32*, 665–667.
- Dubrac, S., and Touati, D. (2002). Fur-mediated transcriptional and post-transcriptional regulation of FeSOD expression in *Escherichia coli*. *Microbiology* *148*, 147–156.
- Emsley, P., Lohkamp, B., Scott, W.G., and Cowtan, K. (2010). Features and development of Coot. *Acta Crystallogr. Sect. D Biol. Crystallogr.* *66*, 486–501.
- Ernst, F.D., Homuth, G., Stoof, J., Mader, U., Waidner, B., Kuipers, E.J., Kist, M., Kusters, J.G., Bereswill, S., and van Vliet, A.H.M. (2005). Iron-responsive regulation of the *Helicobacter pylori* iron-cofactored superoxide dismutase SodB is mediated by Fur. *J. Bacteriol.* *187*, 3687–3692.
- Fillat, M.F. (2014). The fur (ferric uptake regulator) superfamily: Diversity and versatility of key transcriptional regulators. *Arch. Biochem. Biophys.* *546*, 41–52.

Friedman, C.R., Hoekstra, R.M., Samuel, M., Marcus, R., Bender, J., Shiferaw, B., Reddy, S., Ahuja, S.D., Helfrick, D.L., Hardnett, F., et al. (2004). Risk factors for sporadic *Campylobacter* infection in the United States: A case-control study in FoodNet sites. *Clin. Infect. Dis.* 38 Suppl 3, S285–S296.

Gibney, K.B., O'Toole, J., Sinclair, M., and Leder, K. (2014). Disease burden of selected gastrointestinal pathogens in Australia, 2010. *Int. J. Infect. Dis.* 28, 176–185.

Gilston, B. a, Wang, S., Marcus, M.D., Canalizo-Hernández, M. a, Swindell, E.P., Xue, Y., Mondragón, A., and O'Halloran, T. V (2014). Structural and Mechanistic Basis of Zinc Regulation Across the *E. coli* Zur Regulon. *PLoS Biol.* 12, e1001987.

Godschalk, P.C.R., Heikema, A.P., Gilbert, M., Komagamine, T., Ang, C.W., Glerum, J., Brochu, D., Li, J., Yuki, N., Jacobs, B.C., et al. (2004). The crucial role of *Campylobacter jejuni* genes in anti-ganglioside antibody induction in Guillain-Barré syndrome. *J. Clin. Invest.* 114, 1659–1665.

Hantke, K. (1981). Regulation of ferric iron transport in *Escherichia coli* K12: isolation of a constitutive mutant. *Mol. Gen. Genet.* 182, 288–292.

Imlay, J.A., Chin, S.M., and Linn, S. (1988). Toxic DNA damage by hydrogen peroxide through the Fenton reaction in vivo and in vitro. *Science* (80-.). 240, 640–642.

Kaakoush, N.O., Mitchell, H.M., and Man, S.M. (2015). *Campylobacter*. In Molecular Medical Microbiology, Y.-W.T.S.L.P.B.T.-M.M.M. (Second E. Schwartzman, ed. (Boston: Academic Press), pp. 1187–1236.

Lanzilotta, W.N., Schuller, D.J., Thorsteinsson, M. V, Kerby, R.L., Roberts, G.P., and Poulos, T.L. (2000). Structure of the CO sensing transcription activator CooA. *Nat. Struct. Biol.* 7, 876–880.

Lavrrar, J.L., Christoffersen, C.A., and McIntosh, M.A. (2002). Fur-DNA interactions at the bidirectional fepDGC-entS promoter region in *Escherichia coli*. *J. Mol. Biol.* 322, 983–995.

Lee, J.W., and Helmann, J.D. (2007). Functional specialization within the fur family of metalloregulators. *BioMetals* 20, 485–499.

Lewin, A.C., Doughty, P. a., Flegg, L., Moore, G.R., and Spiro, S. (2002). The ferric uptake regulator of *Pseudomonas aeruginosa* has no essential cysteine residues and does not contain a structural zinc ion. *Microbiology* 148, 2449–2456.

Little, C.L., Richardson, J.F., Owen, R.J., de Pinna, E., and Threlfall, E.J. (2008). *Campylobacter* and *Salmonella* in raw red meats in the United Kingdom: Prevalence, characterization and antimicrobial resistance pattern, 2003–2005. *Food Microbiol.* 25, 538–543.

Lloyd, R. V., Hanna, P.M., and Mason, R.P. (1997). The origin of the hydroxyl radical oxygen in the Fenton reaction. *Free Radic. Biol. Med.* 22, 885–888.

Longenecker, K.L., Lewis, M.E., Chikumi, H., Gutkind, J.S., and Derewenda, Z.S. (2001). Structure of the RGS-like domain from PDZ-RhoGEF: Linking heterotrimeric G protein-coupled signaling to Rho GTPases. *Structure* 9, 559–569.

Lovell, S.C., David, I.W., Arendall, W.B., de Bakker, P.I.W., Word, J.M., Prisant, M.G., Richardson, J.S., and Richardson, D.C. (2002). Structure validation by C α geometry: ϕ/ψ and C β deviation. *Proteins Struct. Funct. Genet.* 50, 437–450.

Lovell, S.C., Davis, I.W., Arendall, W.B. 3rd, de Bakker, P.I.W., Word, J.M., Prisant, M.G., Richardson, J.S., and Richardson, D.C. (2003). Structure validation by Calpha geometry: phi,psi and Cbeta deviation. *Proteins* 50, 437–450.

Lucarelli, D., Russo, S., Garman, E., Milano, A., Meyer-Klaucke, W., and Pohl, E. (2007). Crystal structure and function of the zinc uptake regulator FurB from *Mycobacterium tuberculosis*. *J. Biol. Chem.* 282, 9914–9922.

Lucarelli, D., Vasil, M.L., Meyer-Klaucke, W., and Pohl, E. (2008). The metal-dependent regulators FurA and FurB from *Mycobacterium tuberculosis*. *Int. J. Mol. Sci.* 9, 1548–1560.

Malhotra, A. (2009). Tagging for Protein Expression (Elsevier Inc.).

Miller, C.E., Rock, J.D., Ridley, K. a., Williams, P.H., and Ketley, J.M. (2008). Utilization of lactoferrin-bound and transferrin-bound iron by *Campylobacter jejuni*. *J. Bacteriol.* 190, 1900–1911.

Miller, C.E., Williams, P.H., and Ketley, J.M. (2009). Pumping iron: Mechanisms for iron uptake by *Campylobacter*. *Microbiology* 155, 3157–3165.

Mishu, B., Ilyas, a a, Koski, C.L., Vriesendorp, F., Cook, S.D., Mithen, F. a, and Blaser, M.J. (1993). Serologic evidence of previous *Campylobacter jejuni* infection in patients with the Guillain-Barré syndrome. *Ann. Intern. Med.* 118, 947–953.

Mukherjee, P., Ramamurthy, T., Bhattacharya, M.K., Rajendran, K., and Mukhopadhyay, A.K. (2013). *Campylobacter jejuni* in Hospitalized Patients with Diarrhea, Kolkata, India. *Emerg. Infect. Dis.* 19, 1155.

Munshi, S., Hall, D.L., Kornienko, M., Darke, P.L., and Kuo, L.C. (2003). Structure of apo, unactivated insulin-like growth factor-1 receptor kinase at 1.5 Å resolution. *Acta Crystallogr.* 59, 1725–1730.

Ogawa, N., and Biggin, M.D. (2012). High-throughput SELEX determination of DNA sequences bound by transcription factors in vitro. *Methods Mol. Biol.* 786, 51–63.

P. D. Adams, P. V. Afonine, G. Bunkóczki, V. B. Chen, I. W. Davis, N. Echols, J. J. Headd, L.-W. Hung, G. J. Kapral, R. W. Grosse-Kunstleve, A. J. McCoy, N. W. Moriarty, R. Oeffner, R. J. Read, D. C. Richardson, J. S. Richardson, T. C. Terwilliger, P.H.Z. (2010). PHENIX: a comprehensive Python-based system for macromolecular structure solution. *Acta Crystallogr. D*, 213–221.

Pakotiprapha, D., and Jeruzalmi, D. (2014). Crystallization of Protein-DNA Complexes (Chichester: John Wiley & Sons, Ltd.).

Palyada, K., Threadgill, D., and Stintzi, A. (2004). Iron acquisition and regulation in *Campylobacter jejuni*. *J. Bacteriol.* 186, 4714–4729.

Palyada, K., Sun, Y.-Q., Flint, A., Butcher, J., Naikare, H., and Stintzi, A. (2009). Characterization of the oxidative stress stimulon and PerR regulon of *Campylobacter jejuni*. *BMC Genomics* 10, 481.

Pich, O.Q., and Merrell, D.S. (2013). The ferric uptake regulator of *Helicobacter pylori*: a critical player in the battle for iron and colonization of the stomach. *Future Microbiol.* 8, 10.2217/fmb.13.43.

Pohl, E., Haller, J.C., Mijovilovich, A., Meyer-Klaucke, W., Garman, E., and Vasil, M.L. (2003). Architecture of a protein central to iron homeostasis: Crystal structure and spectroscopic analysis of the ferric uptake regulator. *Mol. Microbiol.* 47, 903–915.

Pope, J.E., Krizova, A., Garg, A.X., Thiessen-Philbrook, H., and Ouimet, J.M. (2007). *Campylobacter* Reactive Arthritis: A Systematic Review. *Semin. Arthritis Rheum.* 37, 48–55.

Qin, H.-Y., Wu, J.C.Y., Tong, X.-D., Sung, J.J.Y., Xu, H.-X., and Bian, Z.-X. (2011). Systematic review of animal models of post-infectious/post-inflammatory irritable bowel syndrome. *J. Gastroenterol.* 46, 164–174.

Rhodes, G. (2006). *Crystallography Made Crystal Clear* (Burlington: Elsevier).

Ridley, K.A., Rock, J.D., Li, Y., and Ketley, J.M. (2006). Heme utilization in *Campylobacter jejuni*. *J. Bacteriol.* 188, 7862–7875.

Salloway, S., Mermel, L., Seamans, M., Aspinall, G., Nam Shin, J., Kurjanczyk, L., and Penner, J. (1996). Miller-Fisher syndrome associated with *Campylobacter jejuni* bearing lipopolysaccharide molecules that mimic human ganglioside GD3. *Infect. Immun.* 64, 2945–2949.

Sheikh, M.A., and Taylor, G.L. (2009). Crystal structure of the *Vibrio cholerae* ferric uptake regulator (Fur) reveals insights into metal co-ordination. *Mol. Microbiol.* 72, 1208–1220.

Tiss, A., Barre, O., Michaud-Soret, I., and Forest, E. (2005). Characterization of the DNA-binding site in the ferric uptake regulator protein from *Escherichia coli* by UV crosslinking and mass spectrometry. *FEBS Lett.* *579*, 5454–5460.

Traoré, D.A.K., El Ghazouani, A., Ilangó, S., Dupuy, J., Jacquamet, L., Ferrer, J.-L., Caux-Thang, C., Duarte, V., and Latour, J.-M. (2006). Crystal structure of the apo-PerR-Zn protein from *Bacillus subtilis*. *Mol. Microbiol.* *61*, 1211–1219.

Troxell, B., and Hassan, H.M. (2013). Transcriptional regulation by Ferric Uptake Regulator (Fur) in pathogenic bacteria. *Front. Cell. Infect. Microbiol.* *3*, 1–13.

Van Vliet, A.H.M., Ketley, J.M., Park, S.F., and Penn, C.W. (2002). The role of iron in *Campylobacter* gene regulation, metabolism and oxidative stress defense. *FEMS Microbiol. Rev.* *26*, 173–186.

Voet, D., and Voet, J.G. (2011). *Biochemistry* (New York: John Wiley & Sons, Inc.).

Wooldridge, K., and Vliet, A. Van (2005). Iron transport and regulation. In *Campylobacter Molecular and Cellular Biology*, (Wymondham, UK: Horizon Bioscience), pp. 293–310.

6. Appendices

6.1. Appendix A: The pStrep-CjFur WT Construct

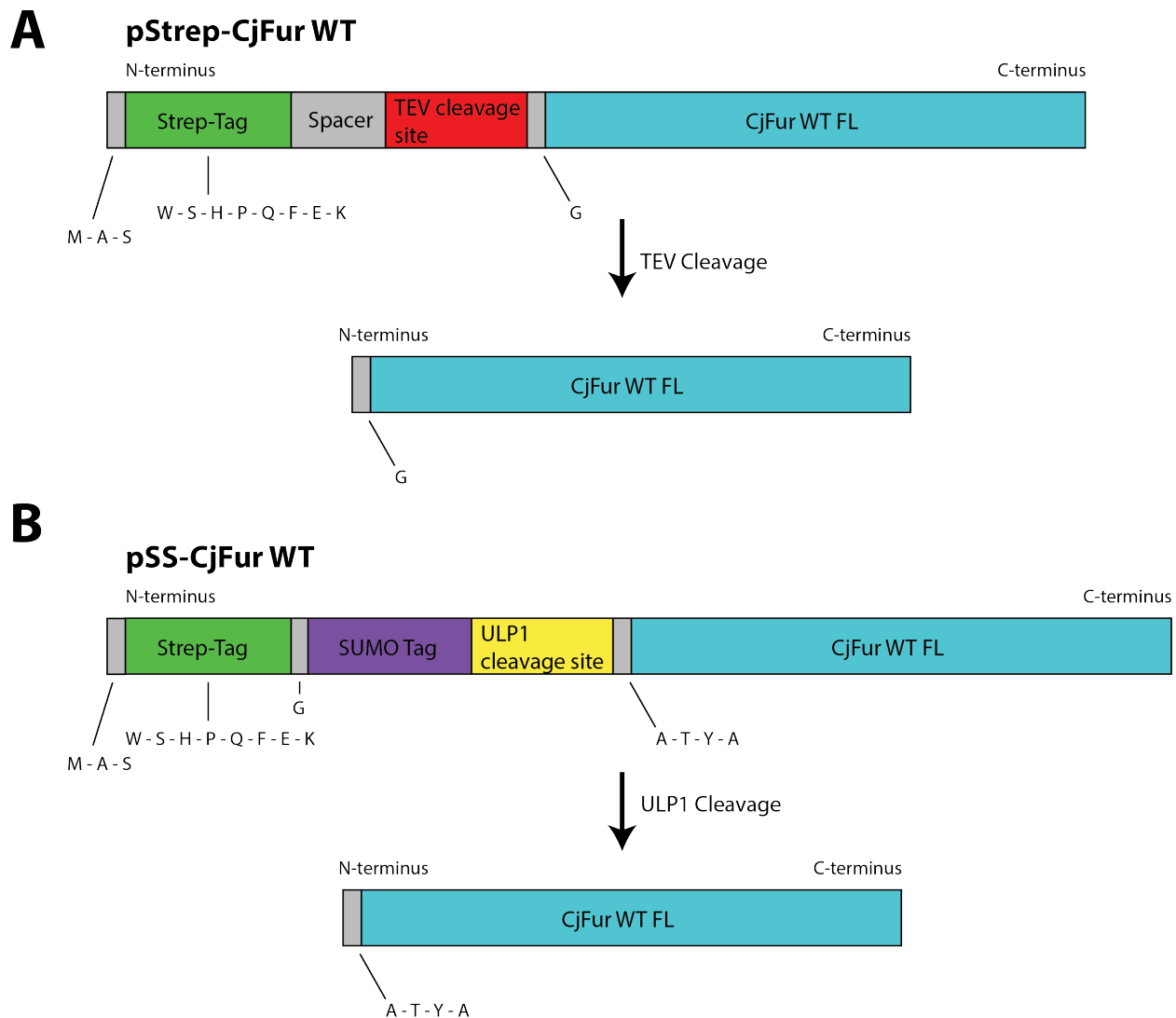


Figure 12. The constructs used to purify and solve the crystal structure of apo-CjFur

This figure illustrates the construct overexpressed and the final crystallizable protein product following cleavage of the tag by a protease. **(A)** The pStrep-CjFur WT construct used for this study is cleaved with TEV and leaves only a Gly residue attached in N-terminal of the WT protein. **(B)** The pSS-CjFur WT construct used in the previous study was cleaved by ULP1 and left an ATYA peptide attached at the N-terminal end of the protein.

6.2.Appendix B: Crystallization of Apo-CjFur

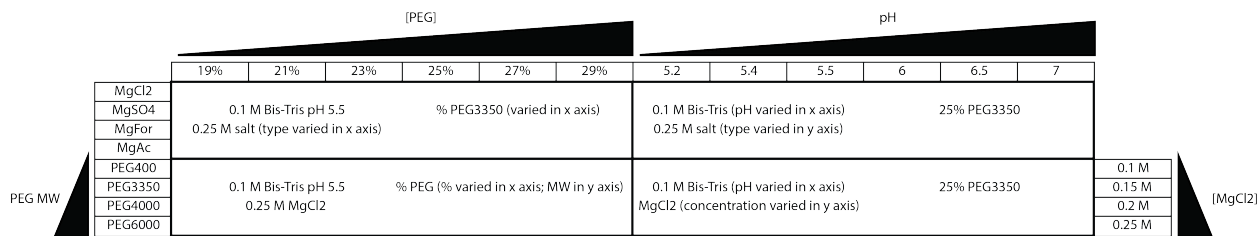


Figure 13. Custom-made crystallization screening kit

A crystallization screening kit was prepared based on conditions that yielded crystals of apo-CjFur previously. Shown are the parameters varied in the crystallization screen.

6.3.Appendix C: Crystallization of the Holo-CjFur-DNA complex

Table 1. List of DNA oligonucleotides screened for the crystallization of the holo-CjFur-DNA complex

The 31 DNA oligonucleotides screened are listed in the table. The sequences belong the *katA* gene promoter region. The top strand is in the 5'->3' orientation, while bottom strand is in the 3'->5' orientation. Flanking ends are shown in CAPS and are excluded from the base pair counts.

| Name | Sequence | Length (bp) |
|------------|--|-------------|
| JFC2390-91 | tgataataaatttcaaaata actattattnaaagtttat | 20 |
| JFC2392-93 | ttgataataaatttcaaaataa aactattattnaaagtttatt | 22 |
| JFC2394-95 | tattgataataaatttcaaaaataat ataactattattnaaagtttattta | 26 |
| JFC2396-97 | ttattgataataaatttcaaaaataatt aataactattattnaaagtttattta | 28 |
| JFC2398-99 | Gattgataataaatttcaaaaataaa taactattattnaaagtttatttC | 24 |
| JFC2400-01 | Gattgataataaatttcaaaaataaa taactattattnaaagtttatttG | 24 |
| JFC2402-93 | GCattgataataaatttcaaaaataaa taactattattnaaagtttatttCG | 24 |
| JFC2414-15 | gtgataataaatttcaaaaata cactattattnaaagtttat | 21 |
| JFC2418-19 | tgataataaatttca actattattnaaagt | 15 |
| JFC2420-21 | ttgataataaatttcaa aactattattnaaagtt | 17 |
| JFC2422-23 | attgataataaatttcaaa taactattattnaaagttt | 19 |
| JFC2432-33 | attgcattttattgataataaatttcaaaaataaaattna taacgtaaaataactattattnaaagtttatttaaatc | 39 |

| | | |
|--------------|---|----|
| JFC2434-35 | ttgcatttattgataataaattcaaaataaattta aacgtaaaataactattattnaagtttatttaat | 37 |
| JFC2436-37 | tgcatttattgataataaattcaaaataaatt acgtaaaataactattattnaagtttatttaat | 35 |
| JFC2438-39 | gcatttattgataataaattcaaaataaatt cgtaaaataactattattnaagtttatttaat | 33 |
| JFC2440-41 | catttattgataataaattcaaaataaatt gtaaaataactattattnaagtttatttaat | 31 |
| JFC2455-56 | Gattgcatttattgataataaattcaaaataaatttag taacgtaaaataactattattnaagtttatttaatC | 39 |
| JFC2457-58 | Gttgcatttattgataataaattcaaaataaattta aacgtaaaataactattattnaagtttatttaatC | 37 |
| JFC2459-60 | Gtgcatttattgataataaattcaaaataaatt acgtaaaataactattattnaagtttatttaatC | 35 |
| JFC2461-62 | Ggcatttattgataataaattcaaaataaatt cgtaaaataactattattnaagtttatttaatC | 33 |
| JFC2463-64 | Gcatttattgataataaattcaaaataaatt gtaaaataactattattnaagtttatttaatC | 31 |
| JFC2467-68 | GGattgcatttattgataataaattcaaaataaatttag taacgtaaaataactattattnaagtttatttaatCC | 39 |
| JFC2469-70 | GGttgcatttattgataataaattcaaaataaattta aacgtaaaataactattattnaagtttatttaatCC | 37 |
| JFC2471-72 | GGtgcatttattgataataaattcaaaataaatt acgtaaaataactattattnaagtttatttaatCC | 35 |
| JFC2473-74 | GGgcatttattgataataaattcaaaataaatt cgtaaaataactattattnaagtttatttaatCC | 33 |
| JFC2475-76 | GGcatttattgataataaattcaaaataaatt gtaaaataactattattnaagtttatttaatCC | 31 |
| JFC2499-2500 | attgcatttattgataataaattcaaaataaatttagGC CGtaacgtaaaataactattattnaagtttatttaatC | 39 |
| JFC2501-2502 | ttgcatttattgataataaattcaaaataaatttaGC CGaacgtaaaataactattattnaagtttatttaaat | 37 |
| JFC2503-2504 | tgcatttattgataataaattcaaaataaatttGC CGacgtaaaataactattattnaagtttatttaaa | 35 |
| JFC2505-2506 | gcatttattgataataaattcaaaataaattGC CGcgtaaaataactattattnaagtttatttaa | 33 |
| JFC2507-2508 | catttattgataataaattcaaaataaattGC CGgtaaaataactattattnaagtttattta | 31 |

Table 2. List of crystallization screening kits used for crystallization experiments

The commercial sparse matrix crystallization screening kits are listed.

| Screening Kit | Manufacturer | Catalog no. |
|--------------------|----------------------|-------------|
| Index screen HT | Hampton Research | HR2-134 |
| Salt screen HT | Hampton Research | HR2-136 |
| Natrix screen HT | Hampton Research | HR2-131 |
| Additive screen HT | Hampton Research | HR2-138 |
| Crystal screen HT | Hampton Research | HR2-130 |
| MCSG-I | Microlytic | MCSG-I |
| MCSG-II | Microlytic | MCSG-II |
| MCSG-III | Microlytic | MCSG-III |
| MCSG-IV | Microlytic | MCSG-IV |
| ProPlex | Molecular Dimensions | MD1-42 |
| Midas | Molecular Dimensions | MD1-59 |
| JCSG I Core Suite | Qiagen | 130924 |

6.4. Appendix D: *In Vitro* Characterization of the CjFur R14E and K17E mutants

The primers used to generate the R14E and K17E mutant are:

For R14E:

Forward:

5' -GTGGAATATGATGTTTACTTGAGGAATTAAAAAAATATTAAGACAAGGC-3'

Reverse:

5' -GCCTTGTCTTAATATTTTAAATTCCCTCAAGTAAAACATCATATTCCAC-3'

For K17E:

Forward:

5' -GATGTTTACTTGAGAGATTAAAGAAATATTAAGACAAGGCGGACTTAAA-3'

Reverse:

5' -TTAAGTCCGCCCTGTCTTAATATTCTTTAAATCTCAAGTAAAACATC-3'

The PCR parameters used for the mutagenesis reaction are:

1 cycle:

95°C (30s)

18 cycles:

95°C (30s)

55°C (1 min)

68°C (10 min)

1 cycle:

68°C (1 min)

Hold at 4°C

The oligonucleotide shifted by CjFur in the EMSA experiments (JFC1588-89) is:

5' -actgaataattgcattttattgataataaatttcaaaataaatttagtttttatatta-3'
3' -tgacttattaacgtaaaataactattattnaaagtttattnaatcaaaaaatataat-5'

from the *katA* gene promoter.